CHALMERS
UNIVERSITY OF TECHNOLOGY

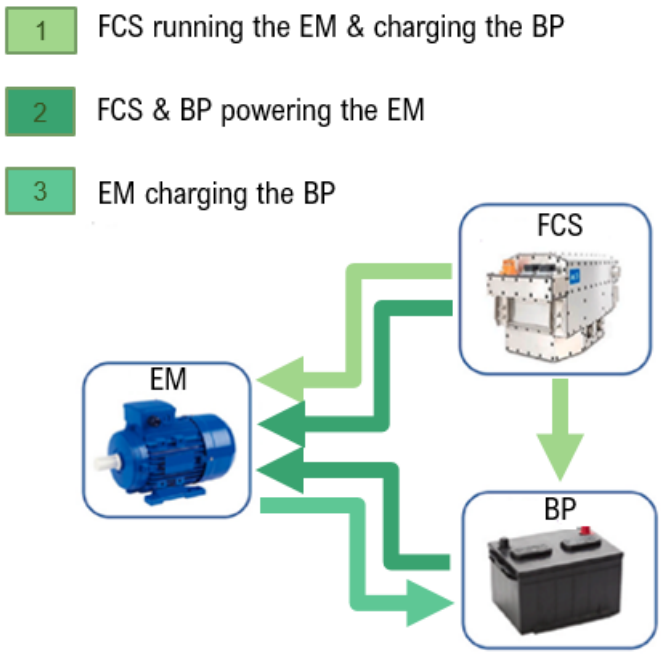

Health Aware Optimisation of the Energy Management of a Fuel Cell – Battery Hybrid Electric Vehicle

Master's thesis in Systems, Control and Mechatronics

EVA SKVOR

DEPARTMENT OF MECHANICS AND MARITIME SCIENCES
Division of Vehicle Engineering and Autonomous Systems

CHALMERS UNIVERSITY OF TECHNOLOGY
Gothenburg, Sweden 2021
www.chalmers.se

MASTER'S THESIS IN SYSTEMS, CONTROL AND MECHATRONICS

Health Aware Optimisation of the Energy Management of a Fuel Cell - Battery Hybrid Electric Vehicle

EVA SKVOR

Department of Mechanics and Maritime Sciences
Division of Vehicle Engineering and Autonomous Systems
CHALMERS UNIVERSITY OF TECHNOLOGY

Göteborg, Sweden 2021

Health Aware Optimisation of the Energy Management of a Fuel Cell - Battery Hybrid Electric Vehicle
EVA SKVOR

Master's thesis 2021:65
Department of Mechanics and Maritime Sciences
Division of Vehicle Engineering and Autonomous Systems
Chalmers University of Technology
SE-412 96 Göteborg
Sweden
Telephone: +46 (0)31-772 1000

Cover:
The cover figure shows the main ways the electric motor (EM), fuel cell system (FCS) and battery pack (BP) interact with one another in a Fuel Cell/Battery Electric Hybrid. (Image adapted from Ma et al. (2021) [27], read more about it in Section 3.1)

Chalmers Reproservice
Göteborg, Sweden 2021

Health Aware Optimisation of the Energy Management of a Fuel Cell - Battery Hybrid Electric Vehicle
Master's thesis in Systems, Control and Mechatronics
EVA SKVOR
Department of Mechanics and Maritime Sciences
Division of Vehicle Engineering and Autonomous Systems
Chalmers University of Technology

Abstract

The background of this thesis is the electric propulsion of heavy electric vehicles and the control problem of the optimal power split between a Lithium-ion battery and a proton-exchange membrane fuel cell system. Both the battery and the fuel cell degrade over time which impacts the resale value as well as the efficiency and life-time of a vehicle. The goal of this thesis is to expand the controller used at Volvo AB to include a cost for this degradation.

Three previous works, Hu et al. (2019) [18], Feng et al. (2020) [13] and Wang et al. (2020) [38], are used as inspiration and to compare and evaluate the results.

The overarching conclusion is that including degradation in the objective function is a sound option that decreases the total cost of ownership and increases the life time of the vehicle. Furthermore, spending some time on formulating good control models to accomplish this is defendable as they, according to this thesis, give better results than simple heuristic limitations on the use.

Besides this, a sound theoretical foundation and a discussion on how the degradation should be modelled is carried out.

Keywords: fuel cells, battery, degradation, optimisation, heavy truck, propulsion

Acknowledgements

I would like to extend my deepest gratitude to my supervisors Olof Lindgärde and Luigi Romano as well as Fredrik Bruzelius and Bengt Jacobsson; your support, guidance and patience throughout my thesis has been invaluable. A special thank you goes out to Erik Jonsson Holm for always answering my questions and reaching out to me with ideas and reflections. I would also like to thank Fatemeh Mohammadi, Qian Xun, Johan Lindberg, Martin Petisme, Anton Klintberg, Björn Wickman and Altaf Faisal for your support as well as Anders Eriksson for giving me the opportunity of doing this thesis at Volvo. Thank you!

Glossary

The abbreviations and definitions used in this thesis may not always match official or more common abbreviations. They are chosen to simplify the narrative of this specific report.

BEV: Battery Electric Vehicle

A plug-in electric vehicle whose powertrain consists of an electric motor and a battery pack.

BP: Battery Pack

Several battery cells connected in series and/or parallel.

Calendar Ageing

Degradation of the battery and fuel cell that occurs due to the passage of time, independently of use.

Controller Model (of Degradation)

A simplified model of the battery and fuel cell degradation, based on their Plant Model used in the objective function of the Modified Power Split Controller.

CV: Conventional Vehicle

A vehicle whose powertrain consists of an internal combustion engine.

ECASA: Electrochemically Active Surface Area

A way to quantify the amount of active platinum (Pt) in the catalyst layer. In order to be able to catalyse the reaction, each Pt nanoparticle needs to be able to come into contact with the reactants. If they e.g clump together (agglomerate), less of the atoms can aid the reaction. This is approximated with an active area; more available Pt corresponds to a larger active area.

EM: Electric Motor

An electrical machine that converts electrical energy into mechanical energy; the electric equivalent to an internal combustion engine.

EMS: Energy Management System

The software responsible for the control of the different powertrain components.

EOL: End-Of-Life

The criterium for when a battery or fuel cell is considered spent, and thrown away.

FC: Fuel Cell Stack

Several fuel cells connected in series.

FCBEV: Fuel Cell-Battery Hybrid Electric Vehicle

An electric vehicle whose powertrain consists of an electric motor, a battery pack and a fuel cell system.

FCEV: Fuel Cell Electric Vehicle

An electric vehicle whose powertrain consists of an electric motor and a fuel cell system.

FCS: Fuel Cell System

The fuel cell stack together with all its auxiliary systems.

HEUR: Heuristic (Power Split) Controller: Original (Power Split) Controller

The Original Power Split controller, provided by Volvo, given by Equations (4.3). It obtains the optimal power vectors for the fuel cell and battery by minimising the H_2-consumption and includes heuristic constraints that limit the fuel cell degradation.

HEV: (Traditional) Hybrid Electric Vehicle

An electric vehicle whose powertrain consists of an internal combustion engine, an electric motor and a battery pack.

Li-ion battery: Lithium-ion battery

Rechargeable batteries that have Lithium ions, Li^+, as positive charge carriers.

Modified (Power Split) Controller

The controller created in this thesis based on the Heuristic Power Split Controller. Two main versions of this controller are examined in this thesis: without degradation (WODGR) and with degradation (WDGR).

MPC: Model Predictive Control

A model predictive controller uses, at each sampling instant, the plant's current input and output measurements, the plant's current state, and the plant's model to calculate, over a finite horizon, a future control sequence that optimises a given performance index and satisfies constraints on the control action. It then uses the first control in the sequence as the plant's input and repeats the process [42].

PEMFC: Proton-Exchange Membrane Fuel Cells

A type of fuel cell that has protons, H^+, as positive charge bearers over a membrane electrolyte.

Plant Model (of Degradation)

A more detailed model of the battery and fuel cell degradation used to calculate the final cost of degradation.

Power Split Controller

The part of the Energy Management System responsible for distributing the power demand between the fuel cell system and the battery pack in a Fuel Cell-Battery Hybrid Electric Vehicle.

QP: Quadratic Programming

The problem of optimising a quadratic objective function (see Section 4.1.1).

SEI: Solid Electrolyte Interface

A thin, solid but permeable layer in the Lithium-ion battery electrolyte that is created and grown by a side-reaction in the battery.

TCO: Total Cost of Ownership

The accumulated monetary cost of owning something, in the case of this thesis, a vehicle.

WDGR: Modified (Power Split) Controller With Degradation

The Modified Power Split controller with degradation, given by Equations (4.10). It obtains the optimal power vectors for the fuel cell and battery by minimising the H_2-consumption and the degradation of electrochemical components.

WODGR: Modified (Power Split) Controller Without Degradation

The Modified Power Split controller without degradation, given by Equations (4.10) using $\alpha = 0$, $\beta = 0$ and $\gamma = 1$ as defined in Equation . It obtains the optimal power vectors for the fuel cell and battery by minimising the cost of H_2-consumption and does not include any heuristic constraints to limit the fuel cell degradation.

Notation

Text Style

To keep a clear, consistent notation, this thesis will use the following:

- blackboard bold text style, $\mathbb{x}$, for optimisation (decision) variables,
- bold text style, $\boldsymbol{b}$, for vectors,
- normal text style, q_{jk} or Q, for constants and constant matrices.

The reason for differentiating between optimisation vectors and "normal" vectors is to easier identify the optimisation variables.

Table of Notation

Table 1: *Table of Notation. Most values are dummy values given in the approximate range of the actual values.*

Notation	Description	Values
$\mathbb{P}_{\text{b}}$, $\mathbb{P}_{\text{b,cell}}$	Optimisation variable for the net power provided by the battery pack and the power provided by a single battery cell [W] Size: $N \times 1$	$\in [P_{\text{b,min}}, P_{\text{b,max}}]$, where $P_{\text{b,max}} > 0$ is the maximal effect the battery can be charged with and $P_{\text{b,min}} < 0$ is the maximal absolute effect the battery can be discharged with.
$\mathbb{P}_{\text{f}}$, $\mathbb{P}_{\text{f,cell}}$, $\Delta\mathbb{P}_{\text{f}}$, $\mathbb{z}_{\text{f}}$	Optimisation variable for the net power provided by the fuel cell system, the power provided by a single fuel cell, the rate change given in Equation (4.3b) and the relaxation variable of its rate change given in Equation (4.7) [W] Sizes: $N \times 1$	For $\mathbb{P}_{\text{f}}$: $\in [P_{\text{f,min}}, P_{\text{f,max}}]$, where $P_{\text{f,max}} > 0$ is the maximal power the fuel cell system can provide and $P_{\text{f,min}} > 0$ is a heuristic minimal power allowed.
$\mathbb{SOC}$	Optimisation variable for the State-of-Charge of the battery pack [-] Size: $(N+1) \times 1$	$\in [0, 1]$, where 1 is a fully charged battery and 0 is an empty battery.
$\mathbb{SOH}_{\text{b}}$, $\mathbb{z}_{\text{b}}$	Optimisation variables related to the State-of-Health of the battery, see Equations (3.10) and (4.8) [-] Sizes: $\mathbb{SOH}_{\text{b}} : (N+1) \times 1$ $\mathbb{z}_{\text{b}} : N \times 1$	For $\mathbb{SOH}_{\text{b}}$: $\in [0.8, 1]$, where 1 is a brand new battery at full health and 0.8 is the battery's State-of-Health at EOL.
$\mathbb{SOH}_{\text{f}}$	Optimisation variables for the State-of-Health of the fuel cell [-] Size: $(N+1) \times 1$	$\in [0, 1]$, where 1 is a brand new fuel cell at full health and 0 is a "dead" fuel cell
$\mathbb{s}$	Slack variable [-]	$\in [0, \infty)$
$\boldsymbol{P}_{\text{ref}}$	The demand (reference) power the battery and fuel cell need to provide for the electric motor or, if negative, the regenerative power the battery should be charged with [W] Size: $N \times 1$	$ca \in [-300000W, 500000W]$

Notation	Description	Values
$\boldsymbol{\Delta t}$	Discrete sampling time interval, see Equation (4.3b) [s] Size: $N \times 1$	ca $\in [0.5, 3]$
N_f, N_p, N_s	Total number of fuel cells in the fuel cell stack, number of parallely and serialy connected battery cells in the battery pack [-]	Withheld from this report.
$P_\mathrm{f,min}$, $P_\mathrm{f,max}$, $P_\mathrm{b,min}$, $P_\mathrm{b,max}$, SOC_min, SOC_max	Minimal and maximal values	$P_\mathrm{f,min} \approx 30000W$ $P_\mathrm{f,max} \approx 270000W$ $P_\mathrm{b,min} \approx -400000W$ $P_\mathrm{b,max} \approx 400000W$ $SOC_\mathrm{min} = 0.15$ $SOC_\mathrm{max} = 0.85$
SOC_i, $SOH_\mathrm{b,i}$, $SOH_\mathrm{f,i}$	The initial State-of-Charge and State-of-Health values	In the MPC framework this value is updated and a part of the input into the Power Split Optimiser, for the runs in this thesis: $SOC_\mathrm{i} = 0.4$ & $SOH_\mathrm{i} = 1$
a_0, a_1, a_2	Second degree approximation constants describing the hydrogen consumption	Withheld from this report.
$\boldsymbol{b}_1$, $\boldsymbol{b}_2$	Linearisation constants for the battery degradation Control Model, see Equation (4.9). Size: 1×4	$\boldsymbol{b}_1 = \begin{bmatrix} 0.85 \cdot 10^{-7} \\ 0.14 \cdot 10^{-5} \\ 0.47 \cdot 10^{-5} \\ 0.17 \end{bmatrix}^T$ $\boldsymbol{b}_2 = \begin{bmatrix} -0.28 \cdot 10^{-4} \\ -0.74 \cdot 10^{-3} \\ -0.29 \cdot 10^{-2} \\ -0.12 \cdot 10^{-1} \end{bmatrix}^T$
c_c, c_s	Heuristic cost factors [-]	$c_\mathrm{r} \approx 10^{-9}$ $c_\mathrm{s} \approx 10^3$
c_f, c_b	Purchase costs for the electrochemical cells [€]	$c_\mathrm{f} = 13487e$ $c_\mathrm{b} = 1848e$
c_H2	Cost of Hydrogen fuel [€/kg]	$c_\mathrm{H2} = 2.8e/kg$
$\alpha_\mathrm{rate,max}$	Heuristic maximal allowed change in $\mathbb{P}_\mathrm{f}$ $[W/s]$	$\alpha_\mathrm{rate,max} \approx 10000W/s$
η_b	Battery efficiency [-]	$\eta_\mathrm{b} \approx 0.95$
Q_nb	Nominal battery capacity, i.e. the amount of charge the battery has stored when fully charged and new [As]	$Q_\mathrm{nb} \approx 150000As$
E_nb	Nominal battery energy [J]	$E_\mathrm{nb} \approx 10^8 J$
c_r	c-rate, i.e. a measure of how fast the battery is charging or discharging, see Equation (3.12) [1/h]	Depends on $\mathbb{P}_\mathrm{b}$
$M(c_\mathrm{r})$	An experimental function for the battery degradation, see Equation (3.11)	$M(c_\mathrm{r}) = 449c_\mathrm{r}^2 - 6301c_\mathrm{r} + 38840$ [18]
$E_\mathrm{a}(c_\mathrm{r})$	Activation energy function [J/mol]	$E_\mathrm{a}(c_\mathrm{r}) = 31700 + 370.3c_\mathrm{r}$ [18]
R	The gas constant [J/(mol K)]	$R = 8.314J/(mol\ K)$
T	Temperature of the battery [K]	$T = 298.15K$
EOL	Battery End-of-Life criterium, see page 8	$EOL = 20\%$
u_nf	Nominal voltage of the fuel cell $[\mu V]$	$u_\mathrm{nf} \approx 0.7\mu V$
γ_low, γ_high, γ_rate	Voltage degradation rates for the fuel cell for low, high and transient (subscript "rate") load	$\gamma_\mathrm{low} = 8.662\mu V/h$ [18] $\gamma_\mathrm{high} = 10\mu V/h$ [18][13] $\gamma_\mathrm{rate} = 0.00004185\mu V/W$ [18]
$f(\mathbb{P}_\mathrm{f,cell})$	A second degree function dictating the fuel cell degradation caused by high or low load	See Model b_f in Figure 4.2.
α, β, γ	Experimental factors, see Equation (4.10a) on page 25.	–

Contents

1 Introduction & Aim

Although there has been a steady overall reduction in greenhouse gas emissions in the EU in recent years, the transport sector has not followed this general trend[1]. An increasingly appealing way to decrease this and other environmental impacts of the sector, is electrification of the vehicle fleet. There are different technologies available to achieve this and Battery Electric Vehicles (BEVs) and Fuel Cell Electric Vehicles (FCEVs) are two of these. Both have drawbacks like low range capacity or slow dynamic response, but these can be mitigated with the hybridisation of both technologies, creating a Fuel Cell-Battery Hybrid Electric Vehicle (FCBEV). The interest in FCEVs (and FCBEVs) has increased in the past decade with research showing a willingness to pay for FCEVs [25][22] and cars like the Toyota Mirai entering the market [14].

Batteries and fuel cells are expensive and suffer from ageing, especially if used in strenuous ways. Prognostics and health management methods can prolong the lifetime and thus reduce the cost of batteries [28] and the same is true for fuel cells [21]. In the case of FCBEVs, a so-called Power Split Controller decides the torque split between the Battery Pack (BP) and the Fuel Cell System (FCS). Traditionally this automatic software only minimises the fuel consumption, but it can be expanded to include the previously mentioned prognostics and health management methods [18] [38] [13]. Taking all these objectives into account (fuel consumption, battery health and fuel cell health) is similar to doing a Total Cost of Ownership (TCO) minimisation where both fuel cost and depreciation, due to e.g. battery and fuel cell wear, are considered.

The aim of this thesis is to reformulate a Power Split Controller used by Volvo to include the cost of degradation of the previously mentioned electrochemical components. The largest focus is on comparing the behaviour of the changed controller with examples of similar applications in literature and determining whether expanding the controller is relevant for further research at Volvo.

1.1 Limitations

The application of the examined software is related to Heavy Duty Long Haul operations which are usually defined as all operations that require a human driver to sleep away from home. Usually such operations are undertaken by heavy vehicles weighing 35-60ton in gross combination weight i.e. the combined weight of vehicle and goods. This thesis, however, limits itself to only investigating a single 90km long cycle and the effect of considering degradation on this short distance. This gives an examined time-horizon of about 1h.

Despite sizing and topology of the investigated vehicle having a large effect on the outcome of the optimisation, they will not be varied in this thesis. The reference vehicle investigated is of the series hybrid architecture type and has a Lithium-ion (Li-ion) BP and a Proton-Exchange Membrane Fuel Cells (PEMFC). Some information about the vehicle and cycle is omitted from this report due to confidentiality reasons.

The degradation models used in this thesis are made to be as simple as possible utilising at most a second degree approximation of the behaviour. Calendar ageing and the effects of degradation on efficiency are for example not included. This is partially due to limiting the scope of the problem, and partially due to the short time-horizon examined in the study (more on this in Section 4).

Thermal processes are also excluded from the degradation model. For the battery the examined literature seems to agree that assuming a constant temperature of ca 25^oC is reasonable. For the fuel cell this simplification is less supported, but, in the examined examples of similar application in literature, basic models of fuel cell degradation also do not include thermal modelling.

For the battery degradation, the definition of the State-of-Health, $\mathbb{SOH}$, used in this report is related to capacity fade and ignores the resistance increase of an ageing battery. While Diao et al. [7] propose an alternative definition of $\mathbb{SOH}$ that takes into account both internal resistance increase

and capacity fade, most of the examined literature still uses the traditional capacity definition, which set the precedent for this thesis.

1.2 Specification of Issue Under Investigation

The following research questions are to be answered:

- How is the degradation of the BP and the FCS to be included in the Power Split Controller?
- How does changing the cost of degradation affect the performance of the vehicle?
- Is including the cost of degradation relevant for future research?

2 Methodology

This thesis uses modelling, simulation and optimisation to obtain results. This is commonplace within the automotive industry, as experiments on real vehicles are often unpractical and expensive.

The software used in this thesis is MATLAB and the openly distributed software YALMIP [26]; a tool for modelling and optimisation in MATLAB.

Models of the relevant processes in the battery and the fuel cell were researched in the literature and discussed with representatives at Volvo, before being included in the model. This should ensure that the included models are up to date with both research (literature) and the industry (Volvo's RnD). Again, due to confidentiality, some details are excluded from this report and if the source of used values of parameters is not explicitly stated in the text, the reader can assume the values are dummy-values not related to Volvo's research.

The Original Controller, the one provided by Volvo, included some heuristic constraints, limiting the behaviour of the fuel cell. The Modified Controller, the one created in this thesis, removes these constraints. To make for an easier analysis and comparison to literature, the Reference Controller, the one other results are compared to was chosen to be the Modified Controller without any of the degradation models and not the Original Controller. In summary, the three most important controllers compared in this thesis are:

- The Original Controller, hereby referred to as HEUR: minimising the H_2-consumption but including heuristic constraints to limit the fuel cell degradation
- The Modified Controller without degradation i.e. The Reference Controller, hereby referred to as WODGR: minimising only the H_2-consumption and not including any heuristic constraints to limit the fuel cell degradation
- The Modified Controller with degradation, hereby referred to as WDGR: minimising the H_2-consumption and the degradation of electrochemical components

A Sensitivity Analysis of the cost-factors is preformed to investigate the effect of the changes made to the code. This is a good way to catch mistakes and to qualitatively explain the effect of including the degradation in the objective function on the overall performance.

3 Theoretical Background

The following is a brief theoretical background on FCBEVs, TCO, the BP and its degradation, the FCS and its degradation and a general overview of the Energy Management System (EMS) of FCBEVs.

3.1 Fuel Cell-Battery Hybrid Electric Vehicles

FCBEVs are vehicles powered by an electric motor that is supplied by electricity from a BP and a FCS. Figure 3.1 shows a schematic sketch of the most important powertrain elements and their interactions.

The biggest commercial hindrance of FCBEVs is the current lack of a hydrogen refuelling infrastructure. Disregarding this, however, the FCBEVs compare favourably to both nonhybrid FCEVs, nonhybrid BEVs and Conventional Vehicles (CVs) in regards to meeting power demands, range and refuelling/charging time [27]. In general, pure FCEVs are rather uncommon; the relatively slow dynamic response and the inability to recover regenerative braking energy, make it challenging to meet the varying power demands of the vehicle. Therefore the FCS is usually combined with either a BP or a super capacitor or both [40]. While the fuel cell stack in the FCEV has difficulties providing sufficient power during acceleration, the battery in a FCBEV hybrid compensates for this. Also, while BEVs need to charge for long periods of time and have a relatively short range before a recharge is needed, the fuel cell system in the hybrid FCBEV compensates for both those issues. This is due to refuelling a H_2-tank taking minutes instead of hours and the high energy density giving the vehicles the longer range. When compared to CVs with internal combustion engines, these two, the range and refuelling-time, are comparable. However, as with the BEV and FCEV, the shorter lifespan of the electrochemical components in the FCBEVs remain a worry, especially when compare to the life time of CVs. Since these components, the battery and the fuel cell, also dominate the monetary cost of the powertrain for a FCBEV [13], examining different ways to extend their lifetime is not only positive from an environmental standpoint but also profitable.

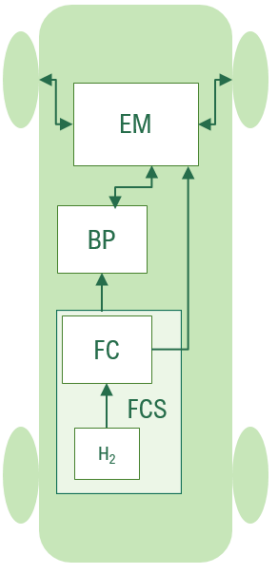

Figure 3.1: *A schematic figure of a FCBEV with the important powertrain elements: the Electric Motor (EM), BP, and the Fuel Cell Stack (FC). Note that the FC needs additional auxiliary systems such as the hydrogen tank (H_2), a compressor, humidifiers, heat exchangers etc. All these together form the FCS (more about this in Section 3.3.2). The direction of the arrows shows the possible flows of energy: both from and to the BP and thus either charging or discharging it, but only from the FCS.*

Besides improving the materials used and other aspects of the technology of batteries and fuel cells, the two main methods used to achieve a longer lifetime of FCBEVs are design optimisation and optimal EMS[18]. The first, design optimisation, includes optimising the sizes of the battery and the fuel cell. FCBEVs on the market today mostly have big fuel cells and small batteries using the battery as a buffering device while letting the fuel cell take a proportionally larger base-load [38]. There are some results by e.g. Feng et al. (2020) [13] that show a bigger battery reduces the cost of the FCS and leads to an overall cost reduction, but this thesis will, as mentioned in 1.1, not investigate the effects of size variation and other design optimisation. The focus, instead, lies on the latter: optimal EMS or, more specifically, the optimal Power Split Controller.

Figure 3.2 is a slightly modified figure from Ma et al. [27]. It shows the main three modes of the EMS of a FCBEV. [27]

It may be worth noting that in a Traditional Hybrid Electric Vehicle

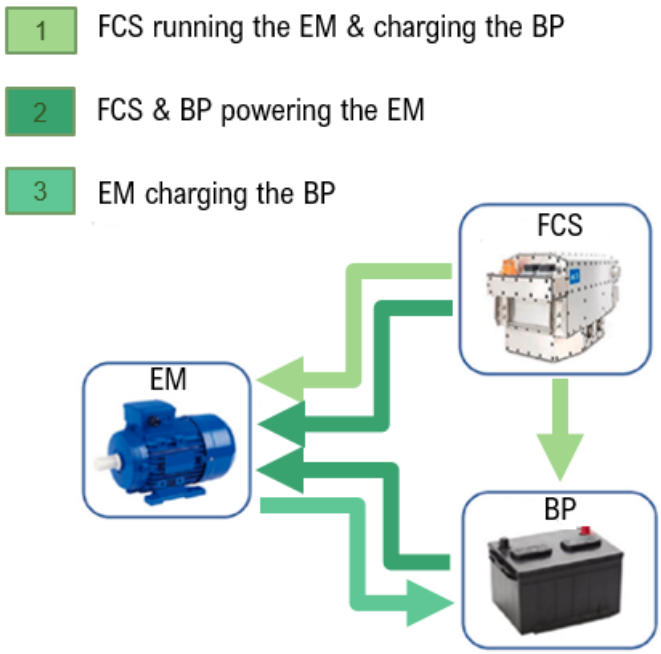

Figure 3.2: *The main ways the EM, FCS and BP interact with one another during an operating cycle. 1: During cruising the FCS provides enough power to both satisfy the power demand from the EM and charge the BP at the same time. 2: During acceleration, the BP helps the FCS meet the changes in power demand from the EM. 3: During braking part of the generated energy from the braking system is used to charge the BP. (Image adapted from Ma et al. (2021) [27])*

(HEV) the distribution of power dictated by the Power Split Controller usually makes the internal combustion engine take care of the dynamic pushes, while the battery functions as a base-load. In fact, one of the reasons for introducing supercapacitors into HEVs is to increase the dynamic output of the electrical system without harming the battery. In a FCBEV the fuel cell takes the role of a base-load, leaving the battery to take care of dynamic changes. This is not optimal for the battery health, so there is research looking at including super capacitors either as a compliment or replacement [40]. According to Xun et al. (2020) [41] electric vehicles with passive hybridisation of fuel cells and supercapacitors have a lower cost and compactness due to the absence of dc-dc converters compared to FCBEVs. As this thesis focuses solely on FCBEVs it does not explore the possible inclusion of supercapacitors.

A way to estimate the cost of the wear on the BP and FC is by using TCO-inspired calculations.

3.2 Total Cost of Ownership

In this thesis TCO is defined as in Ghandriz et al. [16], shown in Equation (3.1).

$$TCO[€] = \underbrace{\text{purchase cost} - \text{resale value}}_{\text{depreciation cost}} + \underbrace{\text{total operational cost}}_{\text{TOC = fuel, maint., tax, ensur. etc}} \tag{3.1}$$

The purchase cost includes the cost of all components, in the case of FCBEVs this would be the FCS, EM and BP but also the tires, the interior of the cabin and the glider. The resale value is usually calculated as a percentage decrease of the purchase value based on an estimation of the wear. The total operational cost includes the cost of fuel consumption and maintenace, as well as tax, ensurance costs, salary of driver etc.

There is research that suggests consumers need to be made more aware of the advantages of a low TCO if electric vehicles are to compete with conventional vehicles. Electric vehicles have a tendency towards higher overall purchase costs, but a much lower operational cost compared to conventional ones. Usually, the price tag of a vehicle only shows the first which can scare away potential costumers.

TCO can have different units depending on the defined problem. $\frac{€}{km}$ is e.g. used by Wu et al. [39] and Kolodziejak et al. [23], while Ghandriz et al. [16] use $\frac{€}{\text{unit freight transported}}$ and Feng et al. [12] use $\frac{€}{year}$.

Depending on the aim of the study the TCO can be simplified to include only relevant costs as in e.g. Kolodziejak et al. [23]. In this thesis the relevant costs would be the purchase costs of the EM, the FCS and the BP. The relevant operational cost would be the cost of the hydrogen fuel and the depreciation value would be a more precise function of the degradation of the electrochemical elements.

3.3 Batteries and Fuel Cells

Both batteries and fuel cells are electrochemical cells, that is devices in which an electrical current is either produced by a spontaneous chemical reaction or used to bring about a nonspontaneous chemical reaction [2]. In essence the process is driven by a redox-reaction between two chemical components, one acting as an electron donor (oxidant), the other as an acceptor (reductant), made to occur over a distance (e.g. two electrodes are separated by an electrolyte) which forces the electrons (and/or ions) to travel and generate a current.

As is common with chemical reactions, this process is far from straight-forward in practice and complicated electrochemical characteristics make both fuel cells and batteries hard to model; there are many nonlinearities and highly dynamic behaviours [28][15]. Broadly speaking, three different possible approaches exist: physics based models, data-driven models and a hybrid combination of both. Physical models give a better understanding of the processes happening and are more general, but they can, especially in the case of batteries and fuel cells, be too complicated and/or take too much computational power to solve [28]. They are also usually based on ideal systems and thus have difficulty capturing real-world losses. The latter is one of the advantages of empirical models: since they are based on real-world data, they automatically include nonidealities. This, however, comes at a high price since purely empirical models need to be reconstructed for each vehicle, road, experiment etc [38]. Thus, usually a hybrid combination of both methods is sought after.

In the examined literature there seems to be a consensus about how to model battery efficiency and degradation, while the same cannot be said about fuel cells. This could be due to the larger commercialisation of BEVs compared to FCBEVs and FCEVs in recent years.

The following Section seeks to lay the basic physical theory of both components with emphasis laid on how their degradation is modelled in the examined literature.

3.3.1 Lithium-ion Batteries

The type of battery examined in this report is the most common rechargeable battery currently on the market, the Lithium-ion (Li-ion) battery. Figure 3.3 shows a schematic of the processes happening when such a battery is used by a load. In the case of this thesis the load would be the EM running on the electrical current provided by the battery.

As always, this is a simplified version of what is happening; in reality there are unwanted bi-reactions and losses due to e.g. mass transport. These losses and non-ideal behaviours are for purposes of energy consumption analysis normally modelled with an equivalent circuit [15]. These can go from simple representations of an ideal voltage source and a single resistor, to more complex representations

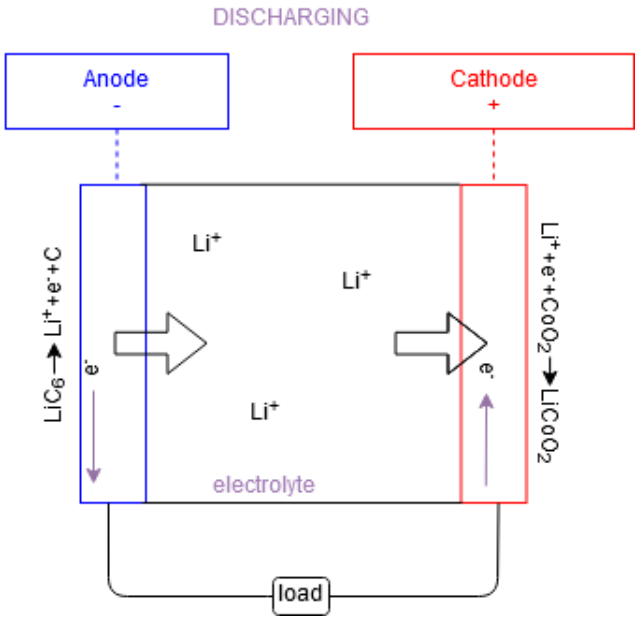

Figure 3.3: *A sketch of the process of discharging a Li-ion battery. A more in depth description of the working of a Li-ion battery can be found in e.g. Zhang et al. (2020) [43], but in essence what is happening is the following: at the anode electrons are stripped from Li-atoms generating a stream of e^- and positively charged Li-ions, Li^+. The former travel through the load to the cathode, generating a current, while the latter travel through the electrolyte to the cathode where they are reunited.*

that consider the dynamic evolution of states. A common equivalent battery circuit is shown in Figure 3.4.

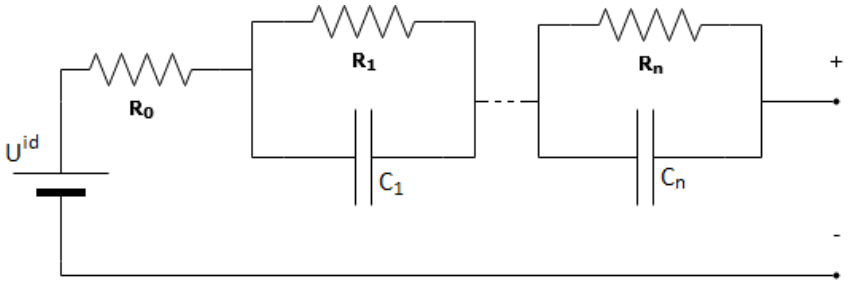

Figure 3.4: *Li-ion Battery equivalent circuit. U^{id} is the ideal battery voltage while R_0 represents losses that are always present in the battery. Depending on how detailed the modelling is, up to n additional losses, depending on the frequency of the current are added. As shown in Equations (3.2), these additional losses are either included in the total impedance of the circuit or not. (Image adapted from [28]).*

As the name implies, the circuit is designed to mimic the behaviour of a battery. U^{id} is the ideal battery voltage and is often denoted OCV for open-circuit-voltage. The values of U^{id}, the resistances $(R_1, ..., R_n)$ and the capacitors $(C_1, ..., C_n)$ need to be experimentally adjusted to the specific battery that is modelled. The values also depend on the State-of-Charge of the battery (see Equation (3.5) for the definition of SOC); in e.g. [38] this dependency is approximated by linear functions. Equations (3.2) demonstrate how the total impedance of the circuit is calculated for an alternating current,

$i(t) = A \cdot \cos(\omega t + \phi)$.

$$\begin{aligned} Z_{\text{Bat,tot}} =& R_0 + Z_1 + ... + Z_\text{n} \\ =& R_0 + \frac{R_1}{1 + j\omega R_1 C_1} + ... + \frac{R_\text{n}}{1 + j\omega R_\text{n} C_\text{n}} \end{aligned} \tag{3.2a}$$

$$\lim_{\omega \to 0} Z_{\text{b,tot}} = R_0 + R_1 + ... + R_\text{n} \tag{3.2b}$$

$$\lim_{\omega \to \infty} Z_{\text{b,tot}} = R_0 \tag{3.2c}$$

As shown in the equations, for low frequencies, i.e. a direct current, the capacitors in the equivalent circuit do not let any current through them, so the current has to go through all the resistors (see Equation (3.2b)). For high frequencies the capacitors instead become equivalent to short-circuits that let all the current through them and thus the only loss happens in R_0 (see Equation (3.2c)), essentially giving an effective voltage $U_\text{eff} = U^{id} - i \cdot R_0$.

In vehicles, many battery cells are combined together to form a battery pack (BP). The pack includes parallel- and serial-connected cells along with the housing and electrical connections. In this thesis N_s denotes how many cells are connected serially and N_p how many are connected paralelly. The total number of cells is obtained by multiplying the two (see Figure 3.5).

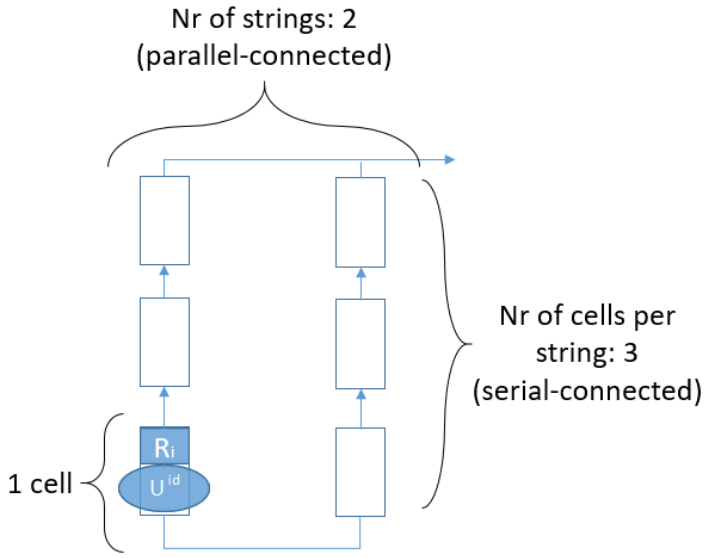

Figure 3.5: *Battery cells in a battery pack. The cells are serial-connected to form multiple parallel-connected strings. The numbers indicated in the figure are arbitrary.*

The ideal electric power one cell can generate is given by $P^{id}_{\text{b,cell}} = U^{id} \cdot i_\text{cell}$. If the cells are assumed to be identical a lumped model of the battery can be assumed which gives the total electric power the battery as shown in Equation 3.3.

$$\boldsymbol{P}^{\boldsymbol{id}}_\text{b} = N_\text{p} \cdot N_\text{s} \cdot \boldsymbol{P}^{\boldsymbol{id}}_{\text{b,cell}} \tag{3.3}$$

$$\mathbb{P}_\text{b} = \eta_\text{b} \cdot P^{id}_\text{b} \tag{3.4}$$

Here the efficiency losses modelled by the equivalent circuit are further simplified into using an efficiency factor η_b. This factor is supposed to take into account both internal losses in the battery and the losses due to transport through wires.

An important concept when modelling batteries is the State-of-Charge of the battery, SOC. SOC is a dimensionless number between 1 and 0 that describes how much charge the battery has at the moment. It is defined as:

$$SOC = \frac{Q_{\text{b, releasable}}}{Q_{\text{nb}}} \tag{3.5}$$

where $Q_{b,releasable}$ is the amount of charge in $[As]$ the battery can release at its current state and Q_{nb} is the nominal battery capacity in $[As]$. If the battery is fully charged and new then $SOC = 1$.

The SOC-rate , i.e. how fast the battery is charged or discharged, is given by:

$$\begin{aligned}\frac{dSOC}{dt} &= \frac{1}{Q_{\text{nb}}} \cdot \frac{dQ_{\text{b, releasable}}}{dt} \\ &= \frac{1}{Q_{\text{nb}}} \cdot \frac{\mathbb{P}_{\text{b}}}{E_{\text{nb}}}\end{aligned}$$

E_{nb} is the nominal battery energy in [J].

Battery Degradation

Batteries age, i.e. their performance degrades throughout their whole life, even if not used. If used strenuously or if treated unkindly by e.g. exposing them to large temperature differences, they age faster. A process often mentioned in the literature relating to battery ageing is the creation and growth of the Solid Electrolyte Interface (SEI). The SEI is created naturally during the first charge of the battery and is a thin solid but permeable layer created by a side-reaction that separates the electrode from the electrolyte. In the beginning it aids the battery, protecting the electrode from corrosion and the electrolyte from reductions, but as it grows it leads to a loss of active surface. Higher temperatures make the SEI dissolve, creating different Li-salts that are less permeable. Lower temperatures instead slow the diffusion of Li^+ through the SEI. More about ageing processes can be found in e.g. Barré et al. (2013) [5].

In relation to the equivalent circuit shown in Figure 3.4, ageing batteries suffer from an increasing internal resistance, R_0, and a decreasing maximal achievable capacity, $Q_{\text{nb,current}}$. The internal resistance essentially relates to how fast the Li^+ can travel through the electrolyte. An increase of internal resistance is thus due to e.g. the creation of passive films around the electrodes and e.g. lower temperatures slowing the diffusion. The capacity instead relates to how much cyclable Li^+ and how much active material is available. The decrease in capacity happens mainly due to different side-reactions where the Li^+ "get stuck". Neither capacity fade nor internal resistance increase are linear in time, even when just considering calendar ageing [5].

The most common way of defining a battery's health is with the State-of-Health function, SOH. There have been two major ways of defining it: with regards to internal resistance and with regards to capacity [4]. The capacity SOH is defined as the ratio of the current capacity to the original rated capacity. The power SOH is defined as the ratio of the difference between the current internal resistance and EOL value and the difference between original rated value and the EOL value. EOL stands for End-of-Life and denotes how old the battery is allowed to be before being discarded, more on this will be explained later. For now, the important thing is that the capacity SOH relates to the battery capacity and the power SOH relates to the internal resistance. Depending on which definition is chosen there may be a difference in the value due to the capacity and internal resistance being independent.

Returning to the equivalent circuit (Figure 3.4), the following equation to describe the output battery power is obtained:

$$\begin{aligned} \boldsymbol{P}_{\mathrm{b}} &= U_{\mathrm{eff}} \cdot i && (3.6)\\ &= (U^{id} - i \cdot Z_{\mathrm{b,tot}}) \cdot i && (3.7)\\ &= U^{id} \cdot i - Z_{\mathrm{b,tot}} \cdot i^2 && (3.8)\\ & && (3.9) \end{aligned}$$

Internal resistance increase leads to a higher $Z_{\mathrm{b,tot}}$ and a capacity decrease affects the U^{id} [35]. Figures 8.1 and 8.2 in the Appendix show the relationship between U^{id} and capacity for a new and old battery and the difference between two batteries with different internal resistances.

One might conclude that the choice between using either capacity or power $\mathbb{SOH}$ should depend on the use of the battery. If used mainly to store energy, the capacity fade seems more important, and since this form of use is common in most everyday electric devices, this process seems to have been more explored in the literature. If, however, used mainly to provide a dynamic "push out" of energy, the increase in internal resistance may be more important.

When it comes to FCBEVs, the role of the battery is, as discussed in 3.1, mainly to provide the system with an extra dynamic shove, meaning the increase in internal resistance seems more important. According to Diao et al. [7], however, it is not quite that simple, as both internal resistance and capacity affects the energy released by a battery pack during the whole discharge process. There is also some evidence to support the claim that internal resistance in Li-ion batteries is much less important than in e.g. Nickel-based batteries [36].

While Diao et al. [7] do propose an alternative definition of $\mathbb{SOH}$ that takes into account both internal resistance increase and capacity fade, this thesis will, as mentioned in 1.1, focus on the capacity $\mathbb{SOH}$. Capacity fade essentially entails that $Q_{\mathrm{b,\ releasable}}$ for an old battery cannot reach Q_{nb} despite being fully charged and will instead only go up to the current maximal limit $Q_{\mathrm{nb,current}}$. The difference between these two is, as mentioned, described by the dimensionless factor $\mathbb{SOH}$, hereby denoted $\mathbb{SOH}_{\mathrm{b}}$ with the subscript b for "battery", defined as:

$$\mathbb{SOH}_{\mathrm{b}} = \frac{Q_{\mathrm{nb,current}}}{Q_{\mathrm{nb}}} \tag{3.10}$$

$\mathbb{SOH}_{\mathrm{b}}$=1 if the battery is new and 0 when it is totally dead. In reality, 0 is almost never reached as batteries are discarded when they reach EOL. In the case of vehicle batteries a usual EOL is 20% which means only a 20% difference between $Q_{nb,current}$ and Q_{nb} is allowed and the batteries are discarded at 80% $\mathbb{SOH}_{\mathrm{b}}$.

A semi-empirical correlation between capacity loss and the discharged [Ah] throughput from [37] is as follows:

$$\boldsymbol{\Delta Q}_{\mathrm{nb}} = M(c_{\mathrm{r}}(\mathbb{P}_{\mathrm{b}})) \cdot \exp\left(\frac{-E_a(c_{\mathrm{r}}(\mathbb{P}_{\mathrm{b}}))}{RT}\right) \cdot A_{\mathrm{tol,dis}}(c_{\mathrm{r}}(\mathbb{P}_{\mathrm{b}}))^z \tag{3.11}$$

This expression describes how the maximal battery capacity deteriorates depending on the usage and temperature. In Equation (3.11) $\boldsymbol{\Delta Q}_{\mathrm{nb}}$ is the difference between $Q_{\mathrm{nb,current}}$ and Q_{nb} in %. R is the gas constant and T is the temperature.

$M(c_{\mathrm{r}})$, $E_a(c_{\mathrm{r}})$ and $A_{\mathrm{tol,dis}}(c_{\mathrm{r}})$ are function of the c-rate, c_{r} in [1/h]=[1C]. c-rate is a measure of how fast the battery is charging or discharging in relation to its maximal capacity. A rate of 1C indicates the current that takes one hour to discharge the battery [15]. Thus the c-rate is defined as follows:

$$
\begin{aligned}
c_{\mathrm{r}}(\mathbb{P}_{\mathrm{b}}) &= \frac{|i_{cell}|}{Q_{\mathrm{nb,cell}} \cdot 3600} \\
&= \frac{|\boldsymbol{P}_{\mathrm{B,cell}}| Q_{\mathrm{nb,cell}}}{Q_{\mathrm{nb,cell}} \cdot 3600 \cdot E_{\mathrm{nb,cell}}} \\
&= \frac{|\mathbb{P}_{\mathrm{b}}|}{3600 N_{\mathrm{p}} N_{\mathrm{s}} E_{\mathrm{nb,cell}}}
\end{aligned} \tag{3.12}
$$

The factor $\frac{1}{3600}$ is included to convert $Q_{\mathrm{nb,cell}}$ from $[As]$ to $[Ah]$.

$M(c_{\mathrm{r}})$, $E_a(c_{\mathrm{r}})$ are an experimental factor and the activation energy respectively, while $A_{\mathrm{tol,dis}}(c_{\mathrm{r}})$, i.e. the tolerated throughput in [Ah] for discharging the battery, is essentially the value of interest: how much can the battery take before it dies.

Using the values in Table 1 and given EOL=20%, Equation (3.11) can be rewritten to:

$$
A_{\mathrm{tol,dis}}(c_{\mathrm{r}}(\mathbb{P}_{\mathrm{b}})) = \sqrt[z]{\frac{\mathrm{EOL}}{M(c_{\mathrm{r}}(\mathbb{P}_{\mathrm{b}})) \cdot \exp\left(\frac{-E_a(c_{\mathrm{r}}(\mathbb{P}_{\mathrm{b}}))}{RT}\right)}} \qquad [Ah] \tag{3.13}
$$

The total throughput in [Ah] is given by both the charged and discharged throughput, i.e. $2A_{\mathrm{tol,dis}}$. Similarily the total available capacity of the battery cell for both discharging and recharging is $2Q_{\mathrm{nb,cell}}$. The number of cycles until EOL, i.e. the number of times the battery can be charged and discharged before EOL, is thus given by the following:

$$
N_{\mathrm{tol}}(c_{\mathrm{r}}(\mathbb{P}_{\mathrm{b}})) = \frac{2A_{\mathrm{tol,dis}}(c_{\mathrm{r}}(\mathbb{P}_{\mathrm{b}}))}{2Q_{\mathrm{nb,cell}} \cdot \frac{1}{3600}} \qquad \left[\frac{Ah}{Ah}\right] \tag{3.14}
$$

$$
\begin{aligned}
&= \frac{3600 \cdot A_{\mathrm{tol,dis}}(c_{\mathrm{r}}(\mathbb{P}_{\mathrm{b}}))}{Q_{\mathrm{nb,cell}}} \\
&= \frac{3600}{Q_{\mathrm{nb,cell}}} \cdot \sqrt[z]{\frac{\mathrm{EOL}}{M(c_{\mathrm{r}}(\mathbb{P}_{\mathrm{b}})) \cdot \exp\left(\frac{-E_a(c_{\mathrm{r}}(\mathbb{P}_{\mathrm{b}}))}{RT}\right)}}
\end{aligned} \tag{3.15}
$$

The time derivative of SOH_b is given by:

$$
\begin{aligned}
\frac{d\$\mathcal{O}\mathbb{H}_{\mathrm{b}}}{dt} &= \frac{1}{Q_{\mathrm{nb,cell}}} \cdot \frac{dQ_{\mathrm{nb,current,cell}}}{dt} \\
&= \frac{1}{Q_{\mathrm{nb,cell}}} \cdot \frac{|i_{cell}(t)|}{2 \cdot N_{\mathrm{tol}}(c_{\mathrm{r}}(\mathbb{P}_{\mathrm{b}}))} \\
&= \frac{1}{Q_{\mathrm{nb,cell}}} \cdot \frac{|\frac{Q_{\mathrm{nb,cell}}}{E_{\mathrm{nb,cell}}} \boldsymbol{P}_{\mathrm{B,cell}}(t)|}{2 \cdot N_{\mathrm{tol}}(c_{\mathrm{r}}(\mathbb{P}_{\mathrm{b}}))} \\
&= \frac{1}{Q_{\mathrm{nb,cell}}} \cdot \frac{Q_{\mathrm{nb,cell}}}{E_{\mathrm{nb,cell}}} \cdot \frac{|\boldsymbol{P}_{\mathrm{B,cell}}(t)|}{2 \cdot N_{\mathrm{tol}}(c_{\mathrm{r}}(\mathbb{P}_{\mathrm{b}}))} \\
&= \frac{|\boldsymbol{P}_{\mathrm{B,cell}}(t)|}{2E_{\mathrm{nb,cell}} N_{\mathrm{tol}}(c_{\mathrm{r}}(\mathbb{P}_{\mathrm{b}}))} \\
&= \frac{|\mathbb{P}_{\mathrm{b}}|}{2N_{\mathrm{p}}N_{\mathrm{s}}E_{\mathrm{nb,cell}} N_{\mathrm{tol}}(c_{\mathrm{r}}(\mathbb{P}_{\mathrm{b}})]} \\
&= \frac{|\mathbb{P}_{\mathrm{b}}|}{2N_{\mathrm{p}}N_{\mathrm{s}}E_{\mathrm{nb,cell}} \frac{3600}{Q_{\mathrm{nb,cell}}} \cdot \sqrt[z]{\frac{\mathrm{EOL}}{M(c_{\mathrm{r}}(\mathbb{P}_{\mathrm{b}})) \cdot \exp\left(\frac{-E_a(c_{\mathrm{r}}(\mathbb{P}_{\mathrm{b}}))}{RT}\right)}}} \\
&= |\mathbb{P}_{\mathrm{b}}| \cdot \frac{1}{2 \cdot 3600 \cdot N_{\mathrm{s}}N_{\mathrm{p}}E_{\mathrm{nb,cell}}} \cdot \frac{Q_{\mathrm{nb,cell}}}{\sqrt[z]{\frac{\mathrm{EOL}}{M(c_{\mathrm{r}}(\mathbb{P}_{\mathrm{b}})) \cdot \exp\left(\frac{E_a(c_{\mathrm{r}}(\mathbb{P}_{\mathrm{b}}))}{R \cdot T}\right)}}}\Bigg)
\end{aligned}
\tag{3.16}
$$

3.3.2 Proton-Exchange Membrane Fuel Cells

The fuel cell examined in this report will be a low Hydrogen Proton-Exchange Membane FCS, (PEMFC). PEMFCs are commonly used in transport applications due to their relatively low operating temperature ($50 - 80^{o}C$), compactness, power density and good efficiency [15]. Figure 3.6 shows the process happening such a fuel cell.

A more in depth description of the workings of a fuel cell can be found in e.g. [32], but Figure 3.6 shows the processes happening in a fuel cell powering a load. Analogous to the battery pack, usually several fuel cells are stringed together and separated with bipolar plates to form the Fuel Cell Stack (FC). In order to function correctly, the FC also needs auxiliary systems such as humidifiers, compressors etc. These are, together with the FC what the term FCS refers to. An example of a FCS is shown in Figure 3.7.

These auxiliary systems make the control of the FCS more complicated to optimise than the battery. The fuel cell response is limited by air feed, H_2 feed, flow regulation, pressure regulation, water management and heat management and controlling it to avoid detrimental degradation means maintaining the optimal temperature, membrane hydration, partial pressure of the reactants etc. [32]

It is also due to all these systems interacting and the relatively slow response of mass flows that the fuel cell has difficulties meeting a dynamic demand and needs to be coupled with either a battery pack or a supercapacitor, as mentioned in Section 3.1.

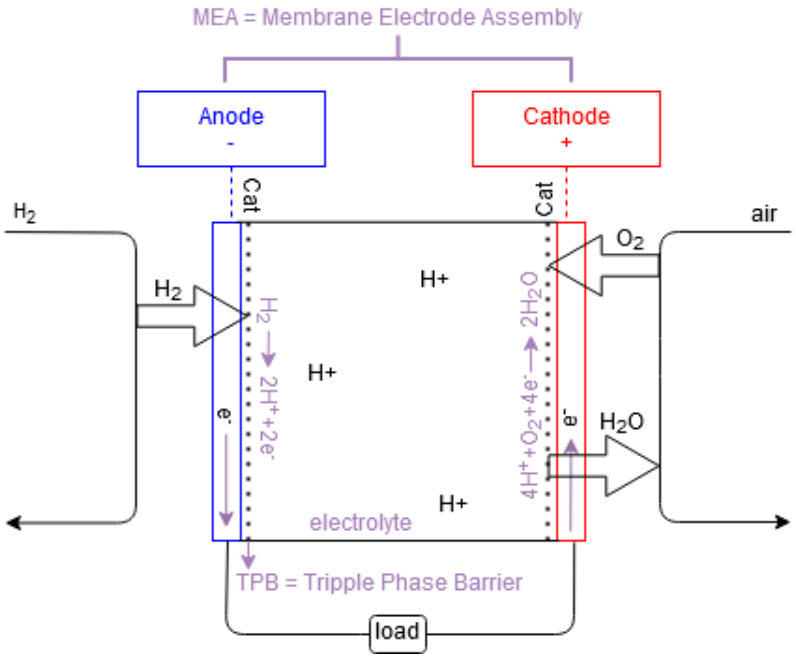

Figure 3.6: *A sketch of the process in a working PEMFC. The hydrogen gas, H_2, is fed into the system and at the anode the Hydrogen atom is stripped of its electron. Similarly to the battery, the electron then travels through the load, generating a current, while the proton (H^+) travels through the electrolyte to the cathode where they are reunited and combined with Oxygen (O_2) to produce water (H_2O). Both electrodes have a catalyst layer (Cat) which aids the process.*

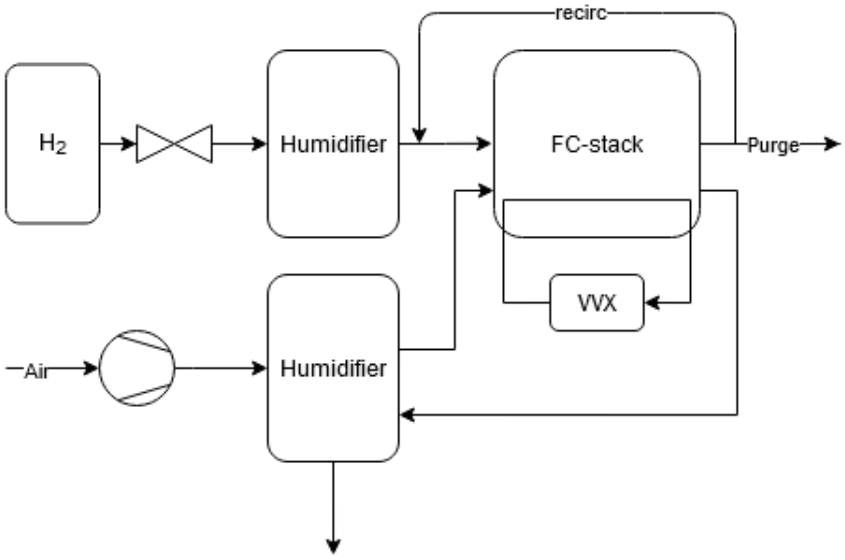

Figure 3.7: *An example of a fuel cell system. The system consists of the H_2-, $air-$, H_2O- and coolant-cycles. The compressor is used to raise the pressure of the inflowing air since a high pressure increases reaction rate. However, increased pressure increases the temperature as well and often the air after the compressor has a too high temperature and has to be cooled [32].*

A fuel cell converts the chemical energy stored in a H_2 molecule to electricity. The total net power the FC can generate, $\mathbb{P}_{\text{fcs}}$, is thus defined as in Equation (3.17).

$$\mathbb{P}_{\mathrm{f}} = \eta_{\mathrm{fcs}} \cdot \boldsymbol{P}_{\mathrm{H2}} - \boldsymbol{P}_{\mathrm{aux}} \tag{3.17}$$
$$= N_{\mathrm{f}} \cdot P_{\mathrm{f,cell}} \tag{3.18}$$

The term $\eta_{\mathrm{fcs}} \cdot \boldsymbol{P}_{\mathrm{H2}}$ denotes how much of the potential chemical energy in the hydrogen gas that is extracted and $\boldsymbol{P}_{\mathrm{aux}}$ denotes how much of the generated fuel cell power needs to go into keeping the fuel cell at the right temperature, humidity etc. N_{f} is the total number of fuel cells in the fuel cell stack.

As with the battery, there have been efforts to model the fuel cell behaviour with an equivalent electric circuit, however there does not seem to be a consensus about the different models in the examined literature. In Runtz et al. (2005) [34] a survey of different fuel cell equivalent circuits is presented.

Either way, the fuel cell operation process has three main types of losses: activation, ohmic and concentration (mass transport) losses [15]. Each of these different losses is dominant in a particular region of current density as shown in Figure 3.8.

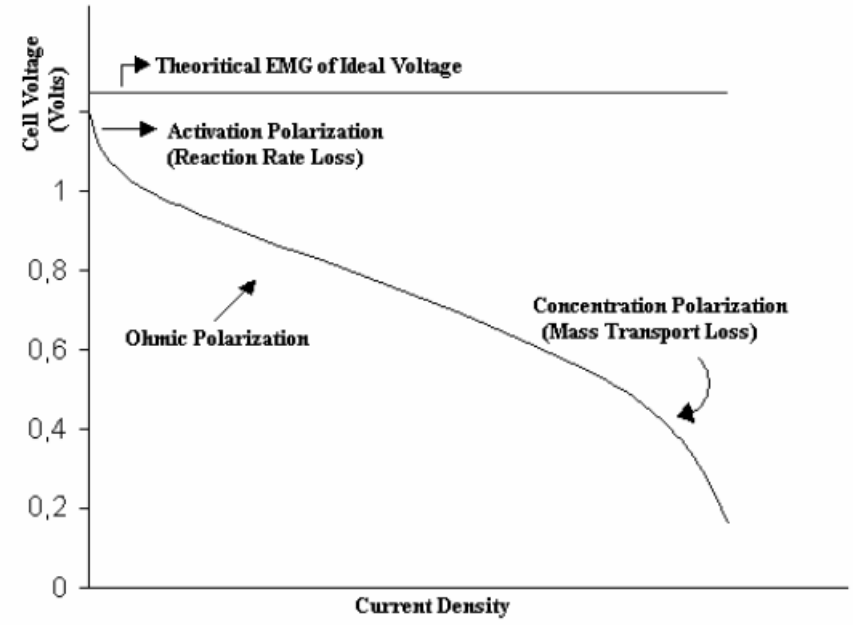

Figure 3.8: *A polarisation curve showing the operating regions of the different losses in fuel cell operation. (Image is adapted from Alexandridis et al. (2008) [24].)*

Before giving a short explanation for each of these losses, let it be said that polarisation curves are essentially graphs plotting fuel cell efficiency for given current densities. The U_{cell} on the y-axis denotes the output voltage from the fuel cell while the current density on the x-axis denotes the demanded output current divided by the area for easier comparison between fuel cells. Ideally, without losses, the cell output voltage would be a constant horizontal line, but for low and high current demands there is a steep, nonlinear deviation from this ideal case, while the middle region is linear.

The activation polarisation loss (dominant at low current density) is present when the rate of the electrochemical reaction at an electrode surface is controlled by sluggish electrode kinetics . [24]

The ohmic loss is due to the resistance of the polymer electrolyte membrane to the ions and the resistance of imperfect electrodes. The loss (voltage drop) in the fuel cell is approximately linear in this region. [24]

The concentration polarisation relates to the change in the concentration of the reactants at the surface of the electrodes as the fuel (hydrogen) is used. The concentrations of the fuel and oxidant are reduced at the various points in the fuel cell gas channels and are less than the concentrations at the inlet portion of the stack. This loss becomes significant at higher currents when the fuel and oxidant are used at higher rates and the concentration in the gas channel is at a minimum. [24]

Fuel Cell Degradation

As with the batteries, there are several different processes that make the fuel cells age, the main ones being catalyst, membrane and gas diffusion layer degradation. An illustrative schematic of different effects from Hu et al. (2020) [18] can be found in the Appendix, but the possibly most important issue is the catalyst degradation relating to the loss of the Electrochemically Active Surface Area (ECASA). The ECASA relates to how much platinum (Pt) is available to aid the required reactions. When fuel cells age, processes like the formation of surface oxides on the electrode, hinder the Pt nanoparticles from coming into contact with the reactants, i.e. the ECASA decreases. Other processes that cause ECASA decay include the corrosion of the electrodes, i.e. carbon oxidation, as the catalyst layer looses its support.

ECASA decay directly increases the activation loss since it makes smaller reaction sites which increases the O_2 mass transfer resistance [38].

The examined literature agrees that the strenuous uses that contribute the most to fuel cell degradation are high load, low load, transient load and start-stop cycles. High load is defined as power demands of 80% and up of the maximal allowed power demand, low load as power demands of 20% and lower of the maximal allowed power demand, transient load as any changes in power demand and start-stop cycles are defined as the number of times the fuel cell is shut down and restarted.

High loads contribute to ECASA decay due to causing a high potential which in turn raises the dissolution rates of the Pt particles. This then leads to a redistribution and agglomeration of the particles [38]. Low loads cause a production of surface oxides which again reduce the ECASA [18]. Start-stop cycles and transient load contribute to the degradation in a process called fuel starvation. This entails that the reactant supply in the fuel cell is insufficient, which causes high overpotential and accelerates the corrosion of the carbon support as well as the agglomeration of the Pt particles. [38][18]

This thesis disregards the effect of start-stop cycles, but it might be relevant for longer horizons.

The sources of degradation are often assumed to be mostly independent and can thus be summed together, as in e.g. Hu et al. (2020) [18].

When modelling the degradation, one way to go about it is by experimentally deciding the degradation rates γ_{low}, γ_{high}, γ_{rate} and γ_{ss}. All the degradation rates are given in relation to the fall in generated fuel-cell voltage in μV, thus I have decided to define $\$\mathcal{OH}_{\text{f}}$ as follows:

$$\$\mathcal{OH}_{\text{f}} = \frac{u_{\text{nf,current}}}{u_{\text{nf}}} \qquad \left[\frac{\mu V}{\mu V}\right] \tag{3.19}$$

Depending on what circumstance the fuel cell is operating at, one of the following expressions for $\Delta\$\mathcal{OH}_{\text{f}} = \$\mathcal{OH}_{\text{f}}[k+1] - \$\mathcal{OH}_{\text{f}}[k]$ hold:

$$\text{Low load: } \Delta t_{\mathrm{L}} \frac{1}{3600} \cdot \frac{\gamma_{\mathrm{low}}}{u_{\mathrm{nf}}} \tag{3.20}$$

$$\text{High load: } \Delta t_{\mathrm{H}} \frac{1}{3600} \cdot \frac{\gamma_{\mathrm{high}}}{u_{\mathrm{nf}}} \tag{3.21}$$

$$\text{Transient load: } |\mathbb{P}_{\mathbb{fcs}}[k+1] - \mathbb{P}_{\mathbb{fcs}}[k]| \cdot \frac{\gamma_{\mathrm{rate}}}{u_{\mathrm{nf}}} \tag{3.22}$$

$$\tag{3.23}$$

Δt_H and Δt_L stand for the amount of time the fuel cell spends under a high or low load. The degradation rates γ are given for a single fuel cell, so a conversion with N_{f} needs to be added.

3.4 The Energy Management Systems of FCBEVs

With two (or more) power sources, coordinating them in a good way becomes very important to ensure both power and cost efficiency [27][15]. Traditionally for CVs and HEVs the main objective is to minimise the fuel (diesel) consumption, since that dominates the cost. When it comes to electric vehicles, however, the cost and resale value of the expensive electrochemical components becomes more important, and thus it becomes important to keep track of their degradation, not only to ensure longevity but also safety[28]. Including degradation costs can effectively extend the lifetime of the FCS at the cost of battery lifetime resulting in a lower TCO [38].

Three papers presenting an EMS for FCBEVs taking into consideration both hydrogen consumption and battery and fuel cell degradation, have been considered in this thesis. These are written by Wang et al. (2019) [38], Hu et al. (2020) [18] and Feng et al. (2020) [13]. They are compared in Table 3.1 with a description of each provided hereafter.

In *Power Management System for a FCBEV Incorporating FC and Battery Degradation* (2019) Wang et al. [38] present an optimisation problem solving for the optimal power split using dynamic programming. The fuel cell degradation is split into degradation caused by start-stop cycles, transient load, idling and high load. The idling part is modelled using a simplified electrochemical of the ECASA decay, i.e. $\mathbb{SOH}_{\mathrm{f}}$ measured as active Pt area decline. High load and transient load are then related to this idling model by assuming roughly linear relationships. Since the analytical solution to the ECASA decay model shows the rate of decay being faster initially, when the FC is new, and then slowing down as the FC ages, the optimal strategy shows the the FC being used more sparingly in the beginning when the decay is bigger, and then more aggressively as the decay levels out. Start and stop is modelled as 3s under a high potential hold. The BP degradation is modelled as capacity loss as presented in Equations 3.11.

The software also includes modelling efficiency as a function of degradation for at least the fuel cell; the same is not mentioned explicitly for the battery. To decrease the computation time the decays are calculated after each step and then applied to the corresponding periods between time points. A new polarisation curve is calculated after each applied step to update the efficiency as a function of degradation.

The shortest cycle length used to evaluate the system is 100h and the longest 5000h.

The results for both show that including degradation in the objective function extends the lifetime of the FC at the cost of BP which gives a lower TCO. When evaluating the shorter horizon of 100h the effect of changing c_{f} is as expected: a low c_{f} gives more transient behaviour for $\mathbb{P}_{\mathrm{f}}$ and more starts and stops, while a high c_{f} keeps the fuel cell power constant at peak fuel efficiency.

The BP degradation costs are small compared to the FC degradation costs and the major differences in cost originate from FC degradation and increasing c_{f} decreases the TCO.

In *Integrated Design and Control Optimization of FCBEV Mining Truck with Minimized Lifecycle Cost* (2020) Feng et al. [13] present a nested optimisation problem solving for both size of the powertrain and the optimal power split. As with Wang et al. the FC degradation is split into start-stop, transient load, idling and high load, but instead of using an analytical model as a base for estimating the degradation, the wear in $[\mu V]$ for the different scenarios is a constant value taken from experiments, e.g. $13.97 \mu V$ per start-stop. The BP degradation is, again, modelled as capacity loss (Equations (3.11)) and efficiency is included as an equivalent circuit for the battery, while the efficiency of the fuel cell is related to P_{aux}.

The software does not include modelling efficiency as a function of degradation, or if it does, it is not stated in the article.

$\$\mathcal{OH}_{\text{f}}$ is indirectly measured as a loss in $[\mu V]$ and $\$\mathcal{OH}_{\text{b}}$ as a quotient of $[Ah]$.

The cycle length used in the analysis of the results is 2000s, i.e. 0.5h, much less than the 100h in Wang et al. Still, even with this short horizon an improvement of the total cost in [$/ton] is achieved when minimising degradation and optimising the size are included in the objective function. The improvement is a result of an increase in BP size and cost to reduce the FC cost and giving a slight improvement to the fuel economy. More specifically, a bigger battery used less aggressively gives about the same battery degradation cost as the original smaller battery used more violently. Both the fuel cell and battery degradation costs per cycle become lower when including degradation in the objective function.

Table 3.1: *A comparison of three papers presenting an EMS for FCBEVs taking into consideration both hydrogen consumption and degradation of the electrochemical components.*

	Wang et al. 2019 [38]	**Hu et al 2020** [18]	**Feng et al. 2020** [13]
Title:	Power management system for a fuel cell/battery hybrid vehicle incorporating fuel cell and battery degradation	Cost-optimal energy mangement of hybrid electric vehicles using fuel cell/battery health-aware predictive control	Integrated design and control optimization of fuel cell hybrid mining truck with minimized lifecycle cost
Battery degradation	Capacity decrease model from Perez et al. 2017[30]	Capacity decrease model from Wang J. et al. 2011 [37]	Capacity decrease model from Wang J. et al. 2011 [37]
FC degradation	start-stop = 3s spent under high potential high load = linear fcn of idling low load = / transient load = linear fcn of idling idle FC = ECASA decay modelled with electro-chemical equations & validated by experiments	start-stop = / (always on) high load = 10 $\frac{\mu V}{h}$ low load = 8.662 $\frac{\mu V}{h}$ transient load = 0.04185 $\frac{\mu V}{kW}$ idle FC = /	start-stop = 13.79 μV high load = 10 $\frac{\mu V}{h}$ low load = / transient load = 0.4185 μV idle FC = 8.662 $\frac{\mu V}{h}$
Solved using:	DP (offline)	SQP and MPC (online)	Nested optimization (offline)
Cycle length:	100h & 5000h	15min	30min
Comments:	The rate of ECSA decay is faster intially: more aggressive control of the FCS later in its life.		Also varies sizing

In *Cost-Optimal Energy Management of HEV Using FC/Battery Helath-Aware Predictive Control* (2020) Hu et al. [18] present an optimisation problem solving for the optimal power split using the MPC framework and sequential QP. The fuel cell is assumed to be "on" the whole time, so the FC degradation model does not account for start-stop cycles. It also does not consider idling separately and introduces degradation for low load. The degradation is modelled similarly to Feng with e.g. a degradation of $10 \frac{\mu V}{h}$ for high power load, same as Feng. The BP degradation is, again, modelled as capacity loss (Equation 3.11).

Efficiency as a function of degradation is not included for the BP or the FC.

The cycle length considered is 1000s, i.e. about 15min, shorter than both Wang and Feng. Over this time the total cost of hydrogen consumption contributes the most. The second largest cost is

the FC degradation cost and the smallest is the BP degradation. The MPC prediction horizon is originally set to 3s and then varied to observe its effect on the total cost. It is concluded that a larger horizon decreases the total cost, but the computation time becomes unsustainable after increasing it over 10s.

To summarise, all examined articles use a capacity fade model for the battery degradation and only Wang et al. include efficiency as a function of degradation in any form. Hu and Feng both use a similar simple way of modelling the fuel cell degradation with experimentally obtained constant degradation rates, while Wang uses a slightly more advanced elecrochemical model. Wang et al. examine the resulting behaviour over the longest cycle, the shortest being 100 hours long, Feng et al. use a cycle of half an hour, while Hu et al. have the shortest cycle of only 15min.

4 Model Formulation

The following Chapter describes the Original Controller and the Modified Controller as well as the Plant and Controller models for the degradation.

4.1 The Original Control System

The original software that this thesis aims to expand upon is a part of a larger system of code tied to simulating predictive vehicle speed control researched at Volvo AB. A simplified schematic of the code structure is shown in Figure 4.1. The Power Split Controller, which is, as mentioned, the focus of this thesis, uses a reference power vector, $\boldsymbol{P}_{\text{ref}}$, as input. $\boldsymbol{P}_{\text{ref}}$ is calculated in the Predictive Vehicle Speed Controller and the trajectory is based on e.g. topography. The goal is to optimise the power control and e.g. make sure to start accelerating before entering an incline of the road so the power needed to transverse it is readily available when starting the incline. $\boldsymbol{P}_{\text{ref}}$ is thus the power the EM needs to meet the optimal speed. The Power Split Controller's job is to split this demand into power that should originate from the battery, $\mathbb{P}_{\text{b}}$, and power that should originate from the fuel cell, $\mathbb{P}_{\text{f}}$. In the simulation this information is then given to a Vehicle Model which approximates the behaviour of a real vehicle. This is all done in a Model Predictive Control (MPC), framework, where an optimal control trajectory over a horizon is updated after applying each step. In this thesis a single horizon, measuring 90km, is examined, with no updating. In the full rendition of the simulation only the first step in this calculated horizon would be applied, the rest would be discarded and a new horizon of 90km would be calculated the next loop, but, for the purpose of this thesis, the resulting trajectory of a single full horizon is considered.

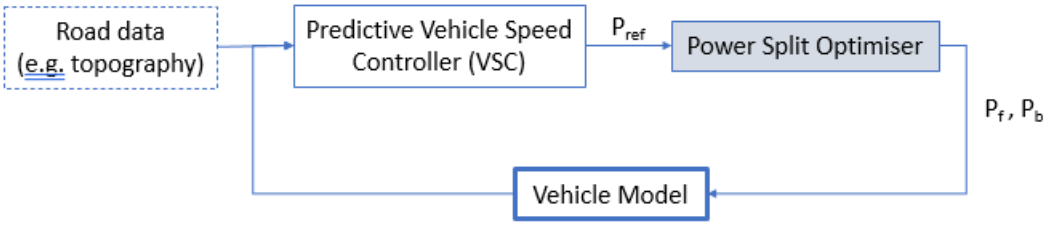

Figure 4.1: *A simplified schematic of the simulating platform used to research predictive speed control at Volvo AB. This thesis focuses on expanding the Power Split Controller (Optimiser) to include degradation of the battery and the fuel cell. Note that only the relevant ingoing and outgoing data is included in the picture.*

4.1.1 Quadratic Programming

HEUR is written in a Quadratic Programming (QP) formulation which will hereby be briefly described. A QP with equality constraints can be written as shown in Equation (4.1).

$$\begin{aligned} \text{min: } & \frac{1}{2}\sum_{j=1}^{n}\sum_{k=1}^{n} q_{jk}x_j x_k + \sum_{j=1}^{n} c_j x_j \\ \text{s.t.: } & \sum_{j=1}^{n} a_{ij}x_j = b_i \qquad (4.1a) \\ & i = 1, ..., m \end{aligned}$$

Written in matrix form this is:

$$\text{min: } \frac{1}{2}\mathbb{x}^T Q\mathbb{x} + \boldsymbol{c}^T\mathbb{x}$$

$$\text{s.t.: } A\mathbb{x} = \boldsymbol{b} \tag{4.2a}$$

As for all nonlinear problems, it is important to know if the problem is convex or not. If it is, each local optimum will also be a global optimum. This is due to most solution methods only guaranteeing to find a local optimum. For the defined QP to be convex, the matrix $Q = (q_{jk})_{n\times n}$ needs to be positive semidefinite.

4.1.2 HEUR: Objective Function and Constraints

HEUR minimises the hydrogen consumption and limits strenuous use of the battery and the fuel cell by applying heuristic constraints on their behaviour. It does not model the ageing of the electrochemical cells or the loss of value and efficiency due to this.

HEUR is defined by Equations (4.3). The variables and parameters introduced are presented in Table 1.

$$\text{Min: } \underbrace{\sum_{k=1}^{N} \boldsymbol{\Delta t}[k] \cdot \left(a_0 + a_1 \cdot \mathbb{P}_\text{f}[k] + a_2 \cdot \mathbb{P}_\text{f}[k]^2\right)}_{H_2 \text{ consumption}} + \underbrace{\sum_{k=1}^{N} c_\text{c} \cdot \Delta\mathbb{P}_\text{f}[k]^2}_{\text{high rate of usage of the FCS}} + \underbrace{c_\text{s} \cdot \mathbb{s}^2}_{\text{slack}} \tag{4.3a}$$

$$\begin{aligned} \Delta\mathbb{P}_\text{f}[k] &= \begin{bmatrix} \mathbb{P}_\text{f}[k+1] - \mathbb{P}_\text{f}[k] \\ 0 \end{bmatrix} \qquad k = 1, ..., N \\ \boldsymbol{\Delta t}[k] &= t[k+1] - t[k] \end{aligned} \tag{4.3b}$$

s.t.:

$$P_{\text{f,min}} \leq \mathbb{P}_\text{f}[k] \leq P_{\text{f,max}} \tag{4.3c}$$

$$P_{\text{b,min}} \leq \mathbb{P}_\text{b}[k] \leq P_{\text{b,max}} \tag{4.3d}$$

$$SOC_\text{min} \leq \mathbb{SOC}[k] \leq SOC_\text{max} \tag{4.3e}$$

$$\mathbb{s} \geq 0 \tag{4.3f}$$

$$\mathbb{SOC}[1] = SOC_\text{i} \tag{4.3g}$$

$$\mathbb{SOC}[N+1] = SOC_\text{i} + \mathbb{s} \tag{4.3h}$$

$$\mathbb{SOC}[k+1] = \mathbb{SOC}[k] - \frac{\boldsymbol{\Delta t}[k]}{E_\text{nb}} \cdot \mathbb{P}_\text{b}[k] \tag{4.3i}$$

$$\mathbb{P}_\text{b}[k] \geq \frac{1}{\eta_\text{b}} \cdot (\boldsymbol{P}_\text{ref}[k] - \mathbb{P}_\text{f}[k]) \tag{4.3j}$$

$$\mathbb{P}_{\mathrm{b}}[k] \geq \eta_{\mathrm{b}} \cdot (\boldsymbol{P}_{\mathrm{ref}}[k] - \mathbb{P}_{\mathrm{f}}[k]) \tag{4.3k}$$

$$\mathbb{P}_{\mathrm{f}}[k] \leq max(\boldsymbol{P}_{\mathrm{ref}}[k] - P_{\mathrm{b,max}} \ , \ P_{\mathrm{f,min}}) \tag{4.3l}$$

$$\left|\mathbb{P}_{\mathrm{f}}[k+1] - \mathbb{P}_{\mathrm{f}}[k]\right| \leq \boldsymbol{\Delta t}[k] \cdot \alpha_{\mathrm{rate,max}} \tag{4.3m}$$

In the introduced QP formulation, the optimisation variable vector is given by:

$$\mathbb{x} = \begin{bmatrix} \mathbb{SOC} \\ \mathbb{P}_{\mathrm{f}} \\ \mathbb{P}_{\mathrm{b}} \\ \boldsymbol{s} \end{bmatrix} = \begin{bmatrix} \mathbb{SOC}[1] \\ \vdots \\ \mathbb{SOC}[N+1] \\ \mathbb{P}_{\mathrm{f}}[1] \\ \vdots \\ \mathbb{P}_{\mathrm{f}}[N] \\ \mathbb{P}_{\mathrm{b}}[1] \\ \vdots \\ \mathbb{P}_{\mathrm{b}}[N] \\ \boldsymbol{s} \end{bmatrix} \tag{4.4}$$

The matrices Q and A can be derived from the objective and constraints given in (4.3) and for the used values, the QP is convex and feasible.

The first part of the Objective (see Equation (4.3a)) i.e. the term describing the H_2 consumption, is a commonly used second degree approximation of the hydrogen mass flow, $[\frac{kg}{s}]$, as a function of $\mathbb{P}_{\mathrm{f}}$. The second term, the cost for high rate of usage of the FCS, is a heuristic punishment on changing the power demand from the fuel cell rapidly. Lastly, the slack variable, $\boldsymbol{s}$, is only used if relaxation of Constraint (4.3h), relating to the final $\mathbb{SOC}$ of the battery, is necessary to obtain feasibility.

Constraints (4.3c) to (4.3h) limit the sizes of the decision variables. Constraint (4.3g) sets the initial value of the State-of-Charge of the battery. In the MPC framework the controller is ultimately a part of, this initial value is updated from the upstream code. Constraint (4.3h) binds the final state-of-charge value close to the initial value. The slack variable, $\boldsymbol{s}$ allows a deviation from this, but at a high cost, which ensures it is only used if the model is close to infeasible. The constraint is needed to ensure the optimiser does not empty the battery within the horizon, i.e. before the whole mission, consisting of several horizons, is finished. The objective function does not have an explicit cost for the battery usage and the whole cycle in the MPC framework is longer than the single horizon explored in this thesis.

Constraint (4.3i) sets the State-of-Charge dynamic.

Constraints (4.3j) and (4.3k) are a relaxation of $\mathbb{P}_{\mathrm{b}}[k] = max(\frac{1}{\eta_{\mathrm{b}}} \cdot (\boldsymbol{P}_{\mathrm{ref}}[k] - \mathbb{P}_{\mathrm{f}}[k]), \eta_{\mathrm{b}} \cdot (\boldsymbol{P}_{\mathrm{ref}}[k] - \mathbb{P}_{\mathrm{f}}[k]))$. They ensure that the power demand is met and that the correct expression for the battery efficiency is taken into account. The former is done by ensuring that $\boldsymbol{P}_{\mathrm{ref}}$ is equal to the sum of the power delivered from the fuel cell and the battery. $\boldsymbol{P}_{\mathrm{ref}}$ can be positive or negative depending on whether the vehicle is braking and the EM wants to charge the battery (negative) or the vehicle is e.g. accelerating and wants either the FCS or the BP or both to deliver energy to the EM (positive). Discharging the battery is less energy efficient that charging it, thus the expression should be $\frac{1}{\eta_{\mathrm{b}}} \cdot \boldsymbol{P}_{\mathrm{ref}}$ when discharging, since $\frac{1}{\eta_{\mathrm{b}}} > \eta_{\mathrm{b}}$. Taking the maximum of both terms ensures this.

Constraint (4.3l) states the following: if $\boldsymbol{P}_{\mathrm{ref}}$ is smaller than $P_{\mathrm{b,max}}$ then the fuel cell should produce as little power as possible. This could occur if the power generated by the braking system would be larger than than the maximal power the battery can safely charge with. In that case the excess power

would need to be burned off somehow and the fuel cell power needs to, as the constraint dictates, be as low as possible to avoid having to burn off even more extra power.

Lastly, Constraint (4.3m) is a heuristic limit on the allowed rate of change of the fuel cell power. This, together with the cost on the high rate usage of the fuel cell in the objective function (4.3a), show that even if this model does not explicitly include modelling the degradation of the electrochemical components, it still includes heuristic rules that limit strenuous use, more specifically, transient load of the fuel cell. Constraints (4.3c) to (4.3e) can also be seen as heuristic limits on both the battery and the fuel cell, since purely physical limitations would set $\mathbb{P}_{\text{f,min}} = 0$, $SOC_{\min} = 0$ and $SOC_{\max} = 1$. Instead, the SOC window is e.g. set between 0.15 and 0.85 and $P_{\text{f,min}}$ is set to 30000W (see Table 1). This seems to be a common practice and, for the SOC window, probably relates not only to the battery degradation but also to the behaviour of the battery being easier to model within this window due to a more linear behaviour.

4.2 The Modified Power Split Controller

A general formulation of the modified objective function is given by Equation (4.5).

Min:

$$\underbrace{\sum_{k=1}^{N} c_{\text{H2}} \cdot \boldsymbol{\Delta t}[k] \cdot \left(a_0 + a_1 \cdot \mathbb{P}_{\text{f}}[k] + a_2 \cdot \mathbb{P}_{\text{f}}[k]^2\right)}_{\text{cost of } H_2 \text{ consumption}} + \underbrace{c_{\text{b}} \cdot (SOH_{\text{b,i}} - \mathbb{SOH}_{\text{b}}[N])}_{\text{cost of battery degradation}} + \underbrace{c_{\text{f}} \cdot (SOH_{\text{f,i}} - \mathbb{SOH}_{\text{f}}[N])}_{\text{cost of fuel cell degradation}} + \underbrace{c_{\text{s}} \cdot \mathbb{s}^2}_{\text{slack}}$$

$$\boldsymbol{\Delta t}[k] = t[k+1] - t[k] \qquad k = 1, ..., N \tag{4.5}$$

Comparing the objectives of the two controllers (Equations (4.3a) and (4.5)), the heuristic term for minimising the change in $\Delta\mathbb{P}_{\text{f}}$ has been removed, while two terms minimising the degradation of the battery and the fuel cell have been added. This formulation is similar to the formulations in Hu et al. (2020) [18] and Feng et al. (2020) [13], and ties in with the TCO calculation used in Kolodziejak (2019) [23], letting the objective be the sum of the fuel consumption cost and the depreciation value of the electrochemical components. Writing the degradation terms in this way makes for an intuitive understanding: the goal is to minimise the difference between the initial State-of-Health and the final State-of-Health. However, since the degradation dynamics are nonlinear, calculations of $\mathbb{SOH}_{\text{b}}[N]$ and $\mathbb{SOH}_{\text{f}}[N]$ need to be simplified to allow for the QP-formulation. Also, the constraints need to be continuous and linear and the dependency on the optimisation variables in the objective function can, at most, be of a second degree.

4.2.1 Control and Plant Models for the Degradation

The modified software uses more detailed Plant Models of the degradation to calculate the degradation after the optimisation has been completed. During the actual optimisation, however, it uses simpler Control Models.

Approximating the Fuel Cell Degradation

Both the Control Model and the Plant Model for the fuel cell degradation are based on the control models used in Feng et al. (2020) [13] and Hu et al. (2020) [18]. Their models are built on knowing the experimental degradation value in μV for high, low and changing values of $\mathbb{P}_{\text{f}}$ (see Section 3.4 for more information). As in Hu et al., the fuel cell is assumed to be "on" the whole time, so no start-stop degradation is taken into account. The values used in this thesis are given in Table 1 and

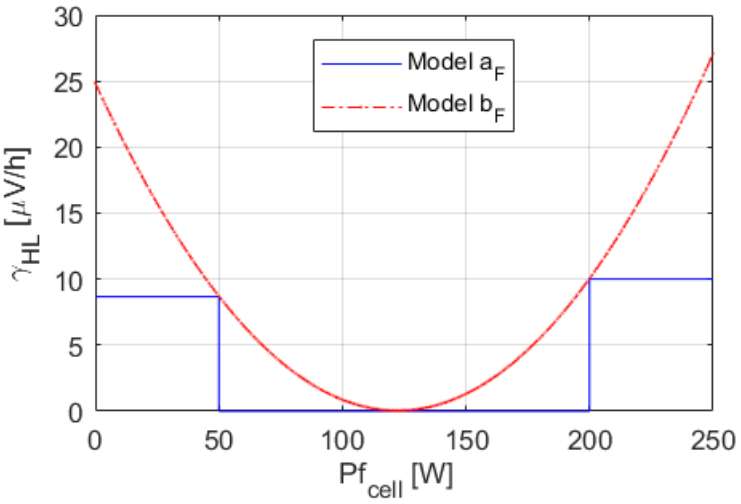

Figure 4.2: *The discrete and the second degree approximation of the fuel cell degradation for high and low $\mathbb{P}_{\mathrm{f}}$. On the x-axis $P_{\mathrm{f,cell}}$ denotes the power for a single fuel cell, i.e. $\mathbb{P}_{\mathrm{f}}/N_{\mathrm{f}}$.*

Figure 4.2 shows the modelling of γ_{low} and γ_{high}. Model a_{F} would be the discrete modelling used by Hu et al., but since the discrete formulation cannot be applied in Quadratic Programming this is used as a Plant Model, while Model b_{F}, a second degree approximation of a_{F} is used as a Control Model.

Using a second degree approximation to model fuel cell degradation has been done before. In Fonesca (2013) [15] a similar application is done, but instead of using changes in μV they use changes in active catalyst surface area. The two are related, but it is easier to measure nominal voltage, than active surface area. Here the State-of-Health of the fuel cell is defined as in Equation (3.19).

The term for the fuel cell degradation given in Equation (4.10a) can be rewritten as shown in Equation (4.6) below.

$$\begin{aligned} c_{\mathrm{f}} \cdot (SOH_{\mathrm{f,i}} - \mathbb{SOH}_{\mathrm{f}}[N]) &= c_{\mathrm{f}} \cdot \sum_{k=1}^{N} \mathbb{SOH}_{\mathrm{f}}[k-1] - \mathbb{SOH}_{\mathrm{f}}[k]) \\ &= c_{\mathrm{f}} \cdot \sum_{k=1}^{N} \underbrace{\left(\frac{\boldsymbol{\Delta t}}{u_{\mathrm{nf}}} \cdot f(\mathbb{P}_{\mathrm{f,cell}}[k]) \right)}_{\text{low \& high load}} + \underbrace{\left(\frac{|\Delta \mathbb{P}_{\mathrm{f,cell}}[k]|}{u_{\mathrm{nf}}} \cdot \gamma_{\mathrm{rate}} \right)}_{\text{transient load}} \end{aligned} \tag{4.6}$$

$$\begin{aligned} \mathbb{SOH}_{\mathrm{f}}[0] &= SOH_{\mathrm{f,i}} \\ \Delta \mathbb{P}_{\mathrm{f,cell}}[k] &= \frac{1}{N_{\mathrm{f}}} \begin{bmatrix} \mathbb{P}_{\mathrm{f}}[k] - \mathbb{P}_{\mathrm{f}}[k-1] \\ 0 \end{bmatrix} \qquad k = 1, ..., N \\ \boldsymbol{\Delta t}[k] &= t[k+1] - t[k] \end{aligned}$$

$f(\mathbb{P}_{\mathrm{f}}[k])$ is the second degree approximation (Model b_{f}). Since absolute values cannot be included in QP formulations, $|\Delta \mathbb{P}_{\mathrm{f}}[k]|$ needs to be relaxed. This is done by introducing a variable $\mathbb{z}_{\mathrm{f}}$ and the following constraints:

$$z_{\mathrm{f}}[0] = 0 \tag{4.7a}$$

$$z_{\mathrm{f}}[k] \geq \frac{\mathbb{P}_{\mathrm{f}}[k]}{N_{\mathrm{f}}} - \frac{\mathbb{P}_{\mathrm{f}}[k-1]}{N_{\mathrm{f}}} \tag{4.7b}$$

$$z_{\mathrm{f}}[k] \geq -\frac{\mathbb{P}_{\mathrm{f}}[k]}{N_{\mathrm{f}}} - \frac{\mathbb{P}_{\mathrm{f}}[k-1]}{N_{\mathrm{f}}} \tag{4.7c}$$

$$z_{\mathrm{f}}[k] \geq 0 \tag{4.7d}$$

$$k = 1, ..., N$$

Since the objective function will be trying to minimise z_{f}, pushing the variable down, while constraints (4.7b) and (4.7c) force z_{f} to be greater than a value, pushing it up, z_{f} ends up being equal to the desired absolute value.

Approximating the Battery Degradation

The Plant Model for the battery degradation used in the modified software is the capacity fade model described in Equation (3.16). The Control Model used in the Power Split Controller is a piece-wise linear approximation of this obtained in the following way.

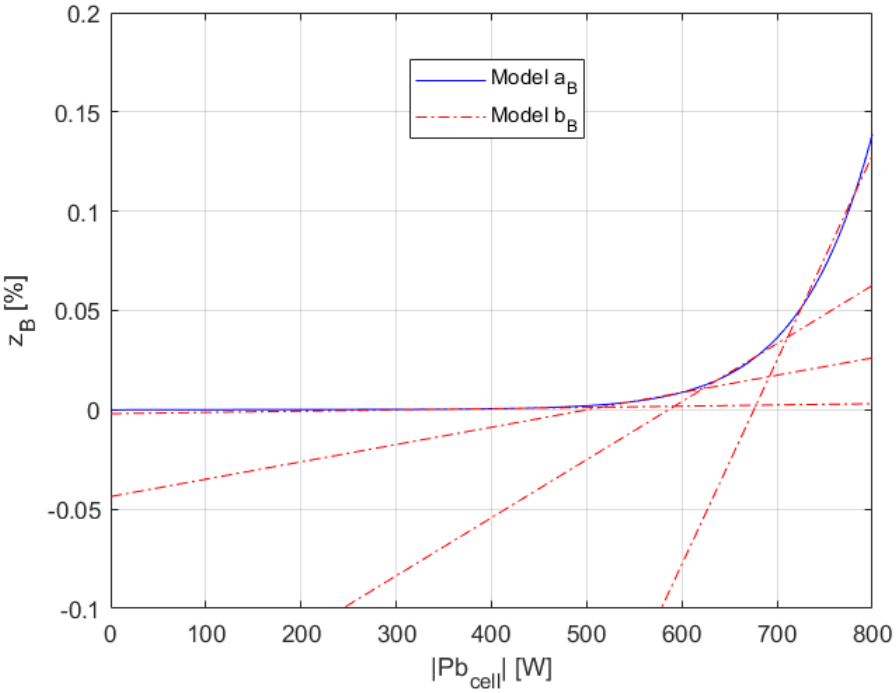

Figure 4.3: *The linear approximation of the battery degradation used in the Modified Controller. For the figure a constant* $\boldsymbol{\Delta t}$ *of 1s has been assumed.*

The term for the battery degradation given in Equation (4.10a) can be rewritten as shown in Equation (4.8).

$$c_{\mathrm{b}} \cdot (SOH_{\mathrm{b,i}} - \$\mathcal{OH}_{\mathrm{b}}[N]) = c_{\mathrm{b}} \cdot \sum_{k=0}^{N} (\$\mathcal{OH}_{\mathrm{b}}[k-1] - \$\mathcal{OH}_{\mathrm{b}}[k]) = c_{\mathrm{b}} \cdot \sum_{k=1}^{N} \mathbb{z}_{\mathrm{b}} \tag{4.8}$$

$\mathbb{z}_{\mathrm{b}}$ is the piece-wise linear approximation of the capacity fade model. In Figure 4.3 the capacity fade model equals Model a_{B} while the linear approximations equal Model b_{B}.

$\mathbb{z}_{\mathrm{b}}$ depends on the c-rate defined in Equation (3.12) and the constraints given in (4.9) give the desired approximation. The absolute value in the definition of the c-rate is relaxed in the same way as the absolute value in Equations (4.7b) and (4.7c) is.

$$\mathbb{z}_{\mathrm{b}} \geq \mathbb{P}_{\mathrm{b,cell}} \cdot \boldsymbol{b}_1 + \boldsymbol{b}_2 \tag{4.9a}$$

$$\mathbb{z}_{\mathrm{b}} \geq -\mathbb{P}_{\mathrm{b,cell}} \cdot \boldsymbol{b}_1 + \boldsymbol{b}_2 \tag{4.9b}$$

$$\mathbb{z}_{\mathrm{b}} \geq 0 \tag{4.9c}$$

4.2.2 Objective Function and Constraints

For convenience sake, the full Modified Power Split Controller with all the constraints in the same place, is given by Equations (4.10) below. Note that many constraints are the same as in HEUR (Equations (4.3)).

Min:

$$\sum_{k=1}^{N} c_{\mathrm{H2}} \cdot \boldsymbol{\Delta t}[k] \cdot \left(a_0 + a_1 \cdot \mathbb{P}_{\mathrm{f}}[k] + a_2 \cdot \mathbb{P}_{\mathrm{f}}[k]^2 \right) + c_{\mathrm{b}} \cdot \sum_{k=1}^{N} \mathbb{z}_{\mathrm{b}} + + c_{\mathrm{f}} \cdot \sum_{k=1}^{N} \left(\frac{\boldsymbol{\Delta t}[k]}{u_{\mathrm{nf}}} \cdot f(\mathbb{P}_{\mathrm{f,cell}}[k]) + \frac{\mathbb{z}_{\mathrm{f}}[k]}{u_{\mathrm{nf}}} \cdot \gamma_{\mathrm{rate}} \right) \tag{4.10a}$$

$$\boldsymbol{\Delta t}[k] = t[k+1] - t[k] \qquad k = 1, ..., N$$

s.t.:

$$P_{\mathrm{f,min}} \leq \mathbb{P}_{\mathrm{f}}[k] \leq P_{\mathrm{f,max}} \tag{4.3c}$$

$$P_{\mathrm{b,min}} \leq \mathbb{P}_{\mathrm{b}}[k] \leq P_{\mathrm{b,max}} \tag{4.3d}$$

$$SOC_{\mathrm{min}} \leq \$\mathcal{OC}[k] \leq SOC_{\mathrm{max}} \tag{4.3e}$$

$$\mathbb{s} \geq 0 \tag{4.3f}$$

$$\$\mathcal{OC}[1] = SOC_{\mathrm{i}} \tag{4.3g}$$

$$\mathbb{SOC}[N+1] = SOC_{\mathrm{i}} + \mathbb{s} \tag{4.3h}$$

$$\mathbb{SOC}[k+1] = \mathbb{SOC}[k] - \frac{\boldsymbol{\Delta t}[k]}{E_{\mathrm{nb}}} \cdot \mathbb{P}_{\mathrm{b}}[k] \tag{4.3i}$$

$$\mathbb{P}_{\mathrm{b}}[k] \geq \frac{1}{\eta_{\mathrm{b}}} \cdot (\boldsymbol{P}_{\mathrm{ref}}[k] - \mathbb{P}_{\mathrm{f}}[k]) \tag{4.3j}$$

$$\mathbb{P}_{\mathrm{b}}[k] \geq \eta_{\mathrm{b}} \cdot (\boldsymbol{P}_{\mathrm{ref}}[k] - \mathbb{P}_{\mathrm{f}}[k]) \tag{4.3k}$$

$$\mathbb{P}_{\mathrm{f}}[k] \leq max(\boldsymbol{P}_{\mathrm{ref}}[k] - P_{\mathrm{b,max}} \ , \ P_{\mathrm{f,min}}) \tag{4.3l}$$

$$\mathbb{z}_{\mathrm{b}} \geq \frac{\mathbb{P}_{\mathrm{b}}}{N_{\mathrm{s}} N_{\mathrm{p}}} \cdot \boldsymbol{b}_1 + \boldsymbol{b}_2 \tag{4.9a}$$

$$\mathbb{z}_{\mathrm{b}} \geq -\frac{\mathbb{P}_{\mathrm{b}}}{N_{\mathrm{s}} N_{\mathrm{p}}} \cdot \boldsymbol{b}_1 + \boldsymbol{b}_2 \tag{4.9b}$$

$$\mathbb{z}_{\mathrm{b}} \geq 0 \tag{4.9c}$$

$$\mathbb{z}_{\mathrm{f}}[0] = 0 \tag{4.7a}$$

$$\mathbb{z}_{\mathrm{f}}[k] \geq \frac{\mathbb{P}_{\mathrm{f}}[k]}{N_{\mathrm{f}}} - \frac{\mathbb{P}_{\mathrm{f}}[k-1]}{N_{\mathrm{f}}} \tag{4.7b}$$

$$\mathbb{z}_{\mathrm{f}}[k] \geq -\frac{\mathbb{P}_{\mathrm{f}}[k]}{N_{\mathrm{f}}} - \frac{\mathbb{P}_{\mathrm{f}}[k-1]}{N_{\mathrm{f}}} \tag{4.7c}$$

$$\mathbb{z}_{\mathrm{f}}[k] \geq 0 \tag{4.7d}$$

A number of different experiments or simulation runs have been performed in this thesis. In the Modified Controller the following α, β and γ in the Objective function have been varied:

$$\text{Min:}$$
$$\gamma \cdot \sum_{k=1}^{N} c_{\mathrm{H2}} \cdot \boldsymbol{\Delta t}[k] \cdot \left(a_0 + a_1 \cdot \mathbb{P}_{\mathrm{f}}[k] + a_2 \cdot \mathbb{P}_{\mathrm{f}}[k]^2 \right) + \alpha \cdot c_{\mathrm{b}} \cdot \sum_{k=1}^{N} \mathbb{z}_{\mathrm{b}} +$$
$$+ \beta \cdot c_{\mathrm{f}} \cdot \sum_{k=1}^{N} \left(\frac{\boldsymbol{\Delta t}[k]}{u_{\mathrm{nf}}} \cdot f(\mathbb{P}_{\mathrm{f,cell}}[k]) + \frac{\mathbb{z}_{\mathrm{f}}[k]}{u_{\mathrm{nf}}} \cdot \gamma_{\mathrm{rate}} \right) \tag{4.10a}$$

The three most important controllers compared in Chapters 5 and 6 are HEUR (given by Equations (4.3)), WDGR (given by Equations (4.10) using $\alpha = 1$, $\beta = 1$ and $\gamma = 1$) and WODGR (given by Equations (4.10) using $\alpha = 0$, $\beta = 0$ and $\gamma = 1$).

In the QP formulation, the optimisation variable vector of the Modified Controller is given by:

$$\mathbb{x} = \begin{bmatrix} \$\mathcal{OC} \\ \mathbb{P}_{\mathrm{f}} \\ \mathbb{P}_{\mathrm{b}} \\ \mathbb{s} \\ \mathbb{z}_{\mathrm{b}} \\ \mathbb{z}_{\mathrm{f}} \end{bmatrix} = \begin{bmatrix} \$\mathcal{OC}[1] \\ \vdots \\ \$\mathcal{OC}[N+1] \\ \mathbb{P}_{\mathrm{f}}[1] \\ \vdots \\ \mathbb{P}_{\mathrm{f}}[N] \\ \mathbb{P}_{\mathrm{b}}[1] \\ \vdots \\ \mathbb{P}_{\mathrm{b}}[N] \\ \mathbb{s} \\ \mathbb{z}_{\mathrm{b}}[1] \\ \vdots \\ \mathbb{z}_{\mathrm{b}}[N] \\ \mathbb{z}_{\mathrm{f}}[1] \\ \vdots \\ \mathbb{z}_{\mathrm{f}}[N] \end{bmatrix} \tag{4.11}$$

The matrices Q and A can be derived from the objective and constraints given in (4.10) and for the used values the QP is convex and feasible.

Cost

For this thesis the purchase cost of H_2 and the electrochemical components was obtained by calculating the average of the values from Wang et al. (2019) [38] and Hu et al. (2020) [18] and converting them to the desired units using the maximal capacity and power output of the battery and fuel cell. See Table 4.1 for more details. The nominal battery capacity and maximal fuel cell power were used to convert from [/kWh] and [/kW].

Table 4.1: *The costs used in this thesis were obtained by averaging the values from Wang and Hu and converting them to the desired units.*

	Wang et al. (2019) [38]	Hu et al. (2020) [18]	This Thesis
H2	2$/kg	4$/kg	2.8€/kg
BP	125$/kWh	178$/kWh	1848.0€
FC	40$/kW	93$/kW	13487.0€

5 Results

This Chapter presents the Results of the thesis.

Due to problems described in Section 6.1, all results presented in this thesis assume the battery degradation is faster than it probably is in reality, skewing the results in the battery's favour.

5.1 Plant vs. Controller Model

Figure 5.2 is a replication of Figure 5.1 from Hu et al. and shows the Number of discharge cycles and the degradation rate given $\mathbb{P}_\mathrm{b}$. As can be seen the replication in Figure 5.2 displays the same behaviour and values as the original. However, when applying the given values from Volvo and mixing them with Hu's values to fill in the missing data, the number of available cycles before EOL goes from the expected 10000 to a mere 3000 and the degradation rate accelerates above $6 \cdot 10^{-7} 1/s$ for lower $\mathbb{P}_\mathrm{b}$ values.

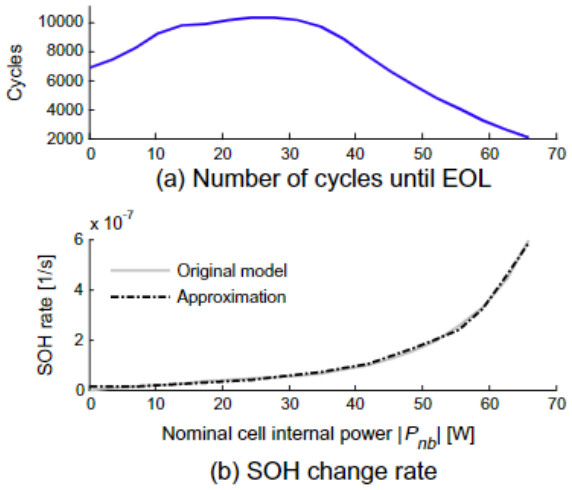

Figure 5.1: *Number of cycles and $\mathbb{SOH}$ change rate from Hu et al. (2020) [18]*

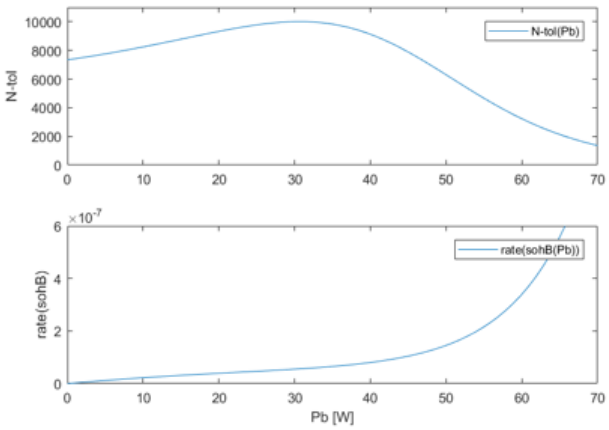

Figure 5.2: *Replication of Figure 5.1 using battery values from Hu et al. (2020) [18].*

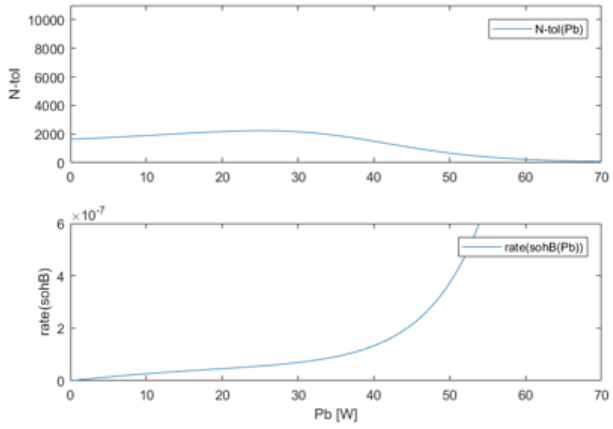

Figure 5.3: *Number of cycles and $\mathbb{SOH}$ change rate mixing battery degradation values from Hu et al. (2020) [18] with values provided by Volvo.*

Figures 5.4 and 5.5 show the difference between $z_{\mathbb{b}}$ and $\mathbb{SOH}_{\mathrm{b}}$ for the Plant and Controller Model for the WODGR.

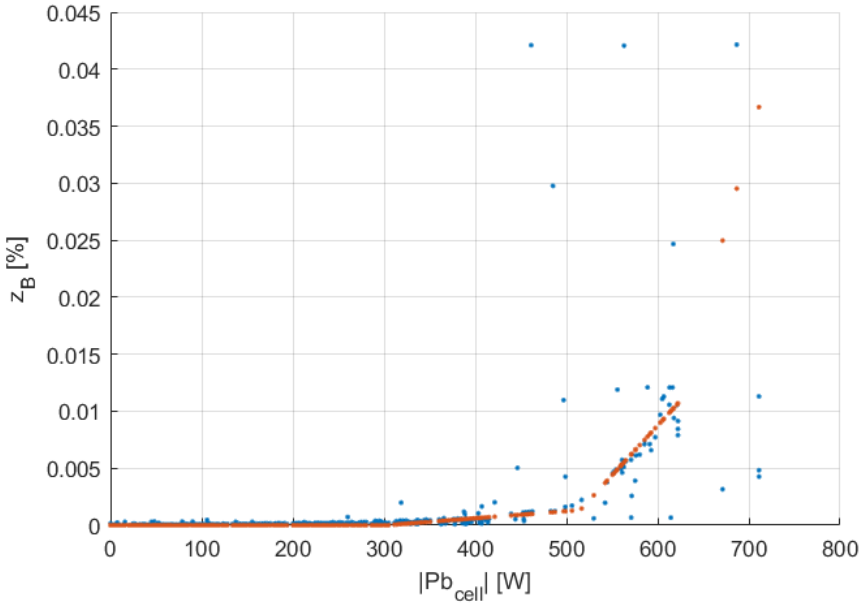

Figure 5.4: *A comparison of $z_{\mathbb{b}} = \mathbb{SOH}_{\mathrm{b}}[k-1] - \mathbb{SOH}_{\mathrm{b}}[k]$ for the capacity fade Plant Model (blue) and the piece-wise linear approximation used in the controller (red). The two models match up well for low absolute values of battery cell power, but deviate for higher values especially between 400-600W.*

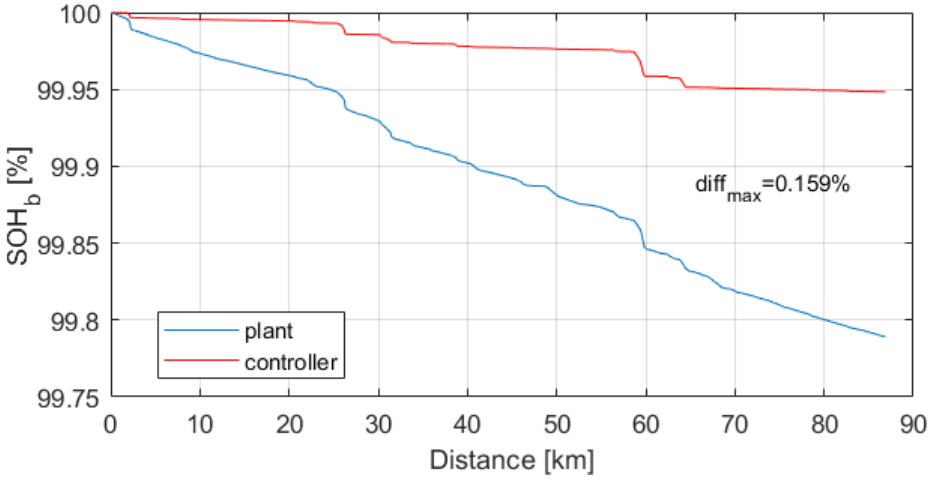

Figure 5.5: *A comparison of the development of $\mathbb{SOH}_{\mathrm{b}}$ over the horizon of 90km for the capacity fade plant model (blue) and the piece-wise linear approximation used in the controller (red). While the resulting accumulated difference of* 0.159% *is disconcerting, it does not affect the the optimal solution (more on this in Section 6.2).*

5.2 Main Results

Table 5.1 shows the main results of experiments performed in this thesis.

Table 5.1: *Comparison of costs for different combination of cost terms. α and β refer to α and β in Equation 4.10a. WDGR has the lowest total cost of all runs, which bodes well for further application of the Modified Controller.*

		BP degr.	FC degr.	Total cost	H_2 cost	BP degr. cost	FC degr. cost
WODGR	$\alpha = 0, \beta = 0, \gamma = 1$	0.83%	0.011%	51.95€	35.02€	15.38€	1.55€
WDGR	$\alpha = 1, \beta = 1, \gamma = 1$	0.21%	0.013%	41.31€	35.73€	3.89€	1.68€
R1	$\alpha = 1, \beta = 1, \gamma = 0$	0.14%	0.004%	89.87€	86.82€	2.55€	0.51€
R2	$\alpha = 1, \beta = 0, \gamma = 1$	0.19%	0.030%	42.89€	35.40€	3.49€	4.00€
R3	$\alpha = 0, \beta = 1, \gamma = 1$	1.39%	0.0001%	60.79€	35.16€	25.61€	0.02€
HEUR		0.83%	0.011%	51.85€	35.03€	15.40€	1.43€

Figures 5.6 and 5.7 show the optimal solution for $\mathbb{P}_\mathrm{b}$, $\mathbb{P}_\mathrm{f}$ and $\$\mathcal{OC}$ plotted against the distance for WODGR and WDGR.

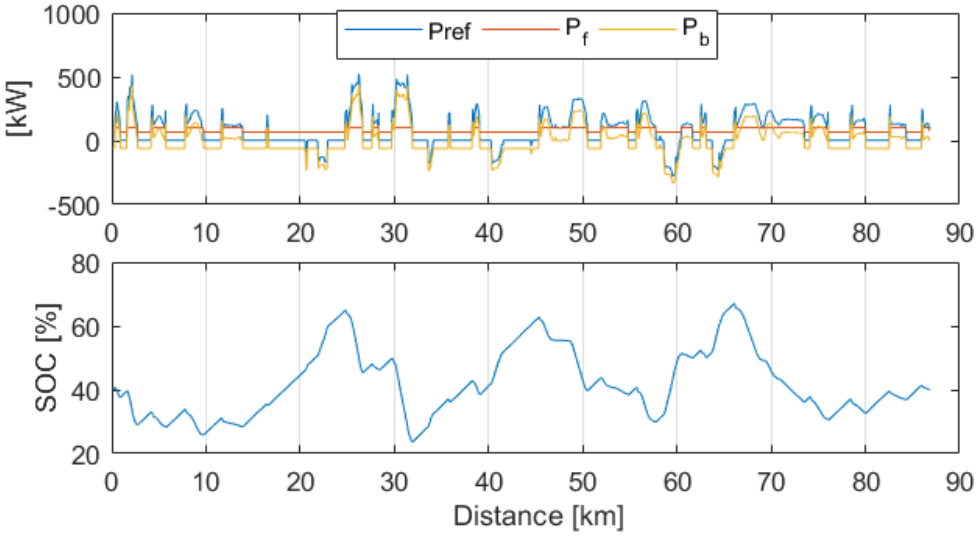

Figure 5.6: *The resulting optimal power split and $\$\mathcal{OC}$ development over the given driving horizon for the WODGR. The first subplot shows $\boldsymbol{P}_\mathrm{ref}$ varying between ca -200kW and 500kW and the sum of $\mathbb{P}_\mathrm{f}$ and $\mathbb{P}_\mathrm{b}$ meeting its demanded value. $\mathbb{P}_\mathrm{f}$ varies between two positive plateaus, while $\mathbb{P}_\mathrm{b}$ varies more. As can be seen in the second subplot, there are three distinctive peaks when the battery is being charged up before releasing its charge.*

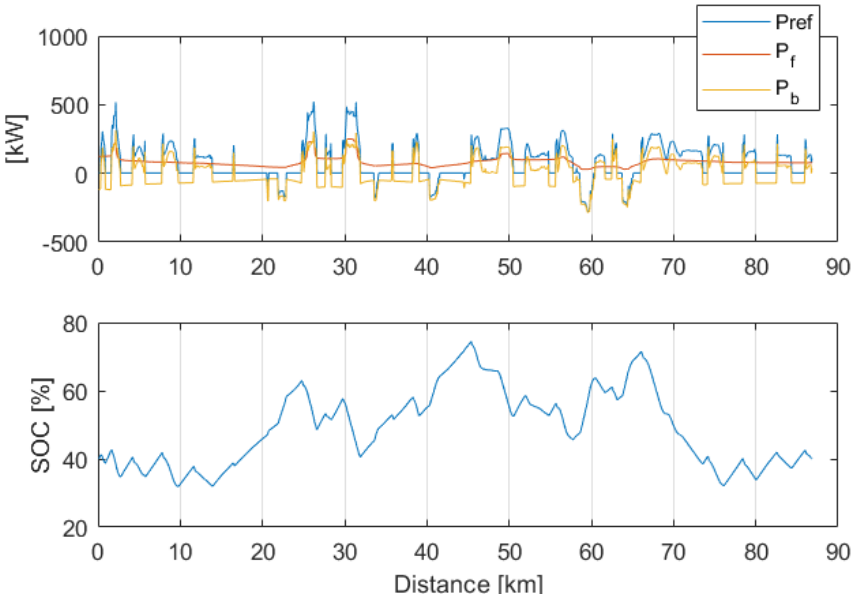

Figure 5.7: *The resulting optimal power split and $\mathbb{SOC}$ development over the given driving horizon for WDGR. The first subplot shows* $\boldsymbol{P}_{\text{ref}}$ *varying between ca -200kW and 500kW and the sum of* $\mathbb{P}_{\text{f}}$ *and* $\mathbb{P}_{\text{b}}$ *meeting its demanded value. As in the WODGR, Figure 5.6,* $\mathbb{P}_{\text{b}}$ *varies more aggressively than* $\mathbb{P}_{\text{f}}$ *and has, as can be seen in the second subplot, three distinctive peaks when the battery is being charged up before releasing its charge. However, comparing* $\mathbb{P}_{\text{f}}$ *for the two runs, the two plateaus mentioned for the WODGR are not as prominent for WDGR; instead* $\mathbb{P}_{\text{f}}$ *has more, softer variations.*

Figures 5.8, 5.9 and 5.10 show the optimal solution for $\mathbb{P}_{\text{b}}$ plotted against $\mathbb{P}_{\text{f}}$ for WODGR, WDGR and HEUR.

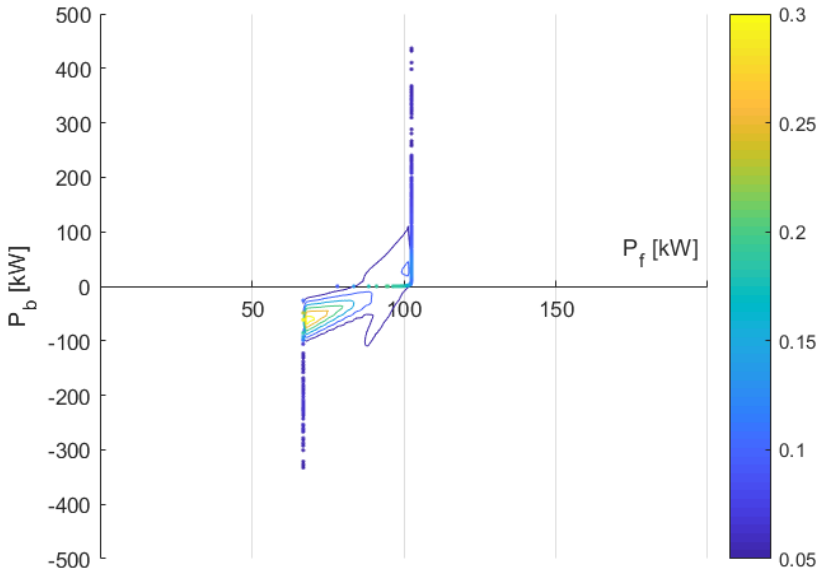

Figure 5.8: *A Density plot for the resulting optimal power split for the WODGR. Yellow shows the most common values for* $\mathbb{P}_{\text{b}}$ *and* $\mathbb{P}_{\text{f}}$*. Negative values for* $\mathbb{P}_{\text{b}}$ *mean the battery is being charged, while positive values mean the battery is being discharged. As seen, the most common arrangement is* $\mathbb{P}_{\text{f}}$ *charging the battery with ca 60kW which happens ca 30% of the time.*

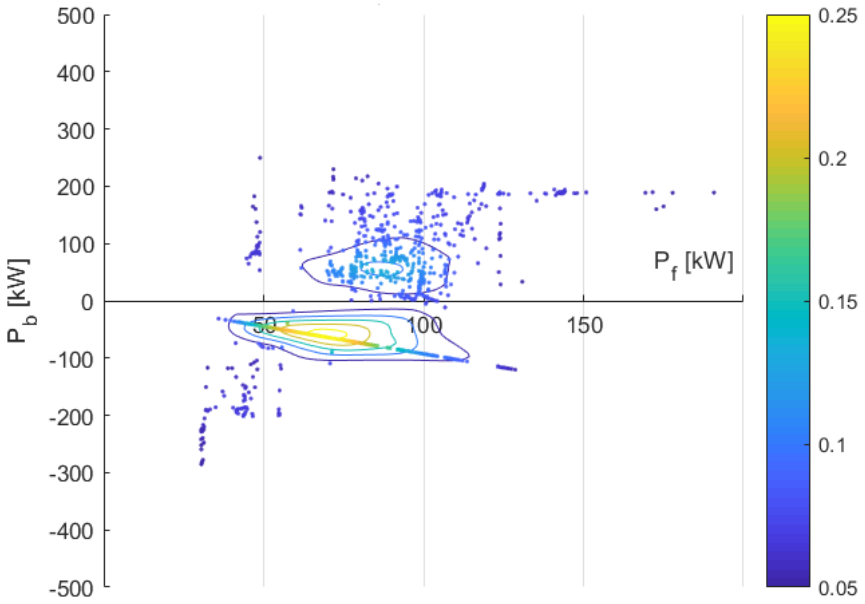

Figure 5.9: *A Density plot for the resulting optimal power split for WDGR. Yellow shows the most common values for $\mathbb{P}_b$ and $\mathbb{P}_f$. Negative values for $\mathbb{P}_b$ mean the battery is being charged, while positive values mean the battery is being discharged. As in the WODGR, Figure 5.8, the most common arrangement is centred around $\mathbb{P}_f$ charging the battery with ca 60kW, but here the region is more smeared out. It is also clear that $\mathbb{P}_f$ behaves differently from the WODGR, lacking the two plateaus at 60kW and 100kW. The maximal and minimal power of the fuel cell are also higher and lower respectively, while the opposite is true for the battery power.*

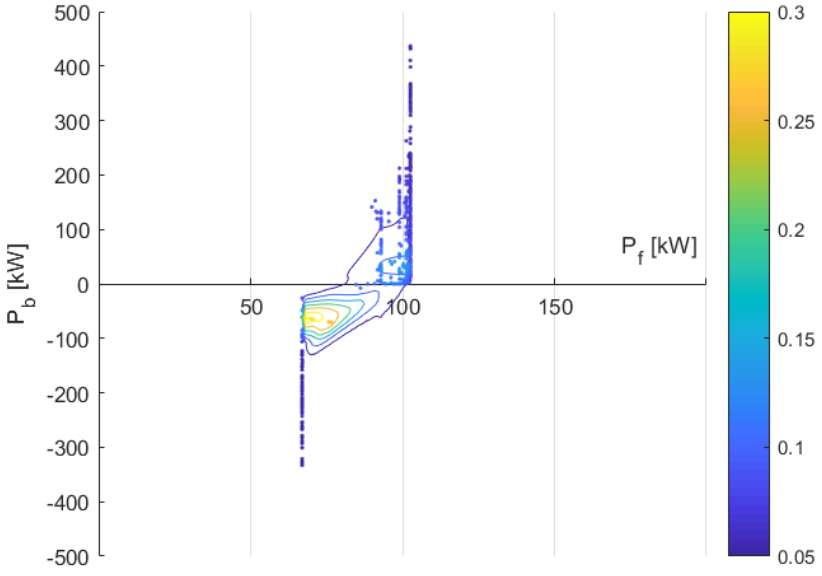

Figure 5.10: *A Density plot for the resulting optimal power split for the Original Controller. Yellow shows the most common values for $\mathbb{P}_b$ and $\mathbb{P}_f$. Negative values for $\mathbb{P}_b$ mean the battery is being charged, while positive values mean the battery is being discharged. The behaviour displayed is very similar to the WODGR of the Modified Controller, Figure 5.8.*

Figures 5.11 and 5.12 compare the WDGR to the WODGR.

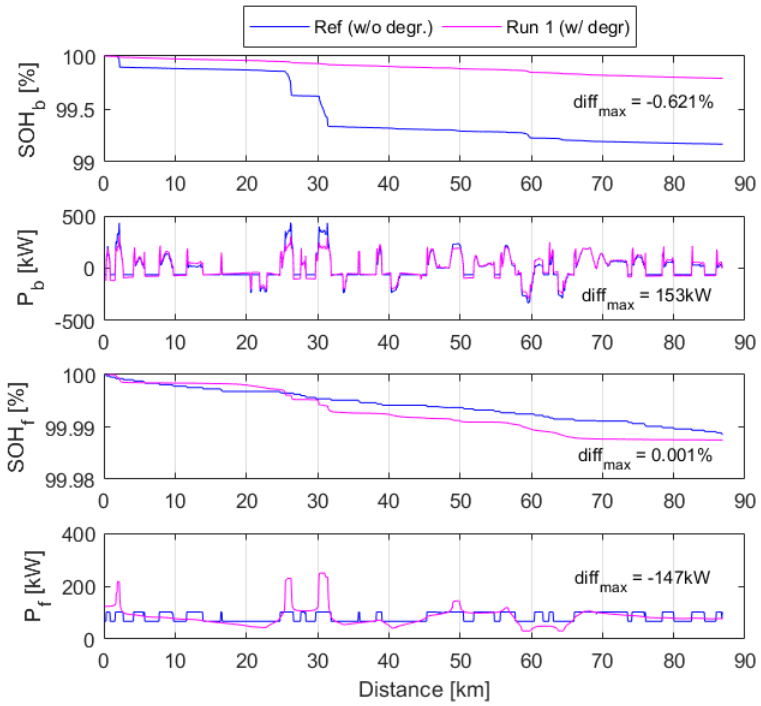

Figure 5.11: *A comparison of the WODGR and WDGR. WDGR has 0.621% lower battery degradation and 0.001% higher fuel cell degradation. The difference in battery and fuel cell power between the two runs is of the same magnitude, ca 150kW. WDGR lowers the battery peak power and sets a higher fuel cell peak power.*

Figures 5.12 and 5.13 show the transients of the optimal $\mathbb{P}_{\mathrm{b}}$ and $\mathbb{P}_{\mathrm{f}}$ for WDGR, WODGR and HEUR.

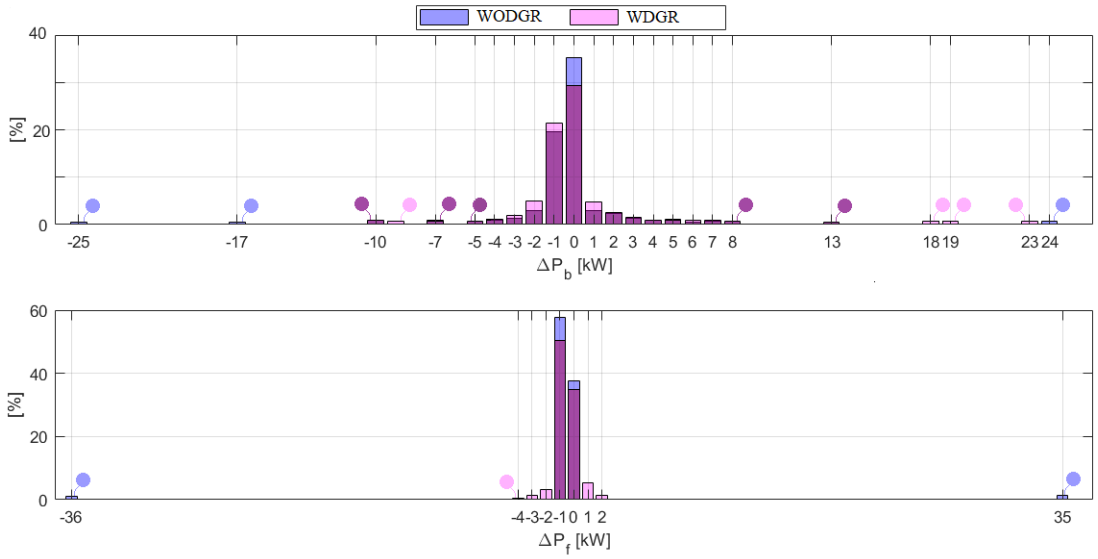

Figure 5.12: *Comparison of the frequency of the transients for $\mathbb{P}_{\mathrm{b}}$ and $\mathbb{P}_{\mathrm{f}}$. The areas where both overlap are in purple. For the battery one can observe that while the overall behaviour is similar, WDGR has $\mathbb{P}_{\mathrm{b}}$ constant, i.e. $\Delta\mathbb{P}_{\mathrm{b}} = 0$, less often than the WODGR, but overall the behaviour is similar. For the fuel cell, as has already been mentioned, WDGR introduces more smaller transients of ca $\pm 3kW$. It also removes the bigger transients of ca $\pm 35kW$. Note that this figures shows ΔP on the x-axis, i.e. the frequency of the transients $P[k+1] - P[k]$ and is thus different from the data in the Density plots which show the frequency of P having a certain value, but does not capture the size of the transients.*

Figure 5.13 shows the frequency of the transients for HEUR.

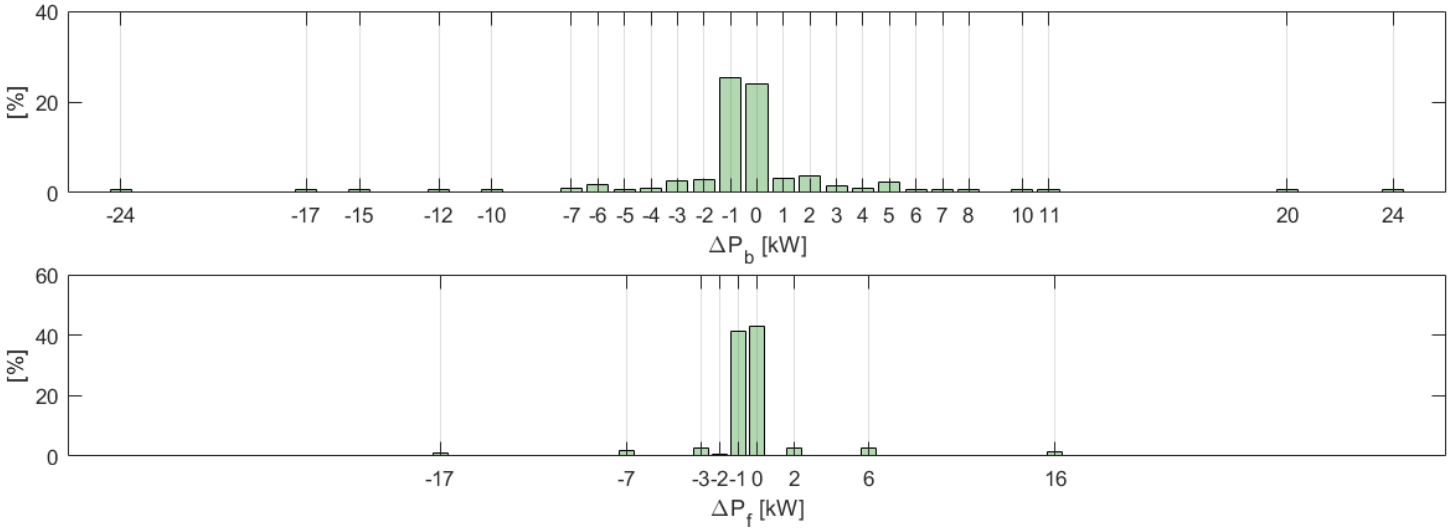

Figure 5.13: *The frequency of the transients for $\mathbb{P}_\mathrm{b}$ and $\mathbb{P}_\mathrm{f}$ for the optimal solution of the HEUR. Compared to the Modified Controller (see Figure 5.12) the Original controller has the highest percentage of $\Delta\mathbb{P}_\mathrm{b} = -1kW$ and $\Delta\mathbb{P}_\mathrm{f} = 0kW$. Note that this figures shows $\Delta\mathbb{P}$ on the x-axis, i.e. the frequency of the transients $\mathbb{P}[k+1] - \mathbb{P}[k]$ and is thus different from the data in the Density plots which show the frequency of P having a certain value, but does not capture the size of the transients.*

Figure 5.14 compares the optimal solution for $\mathbb{P}_\mathrm{b}$ and $\mathbb{P}_\mathrm{f}$ plotted against the distance for the WDGR, WODGR and the experimental runs R1, R2 and R3 (see Table 5.1 for information on R1, R2 and R3).

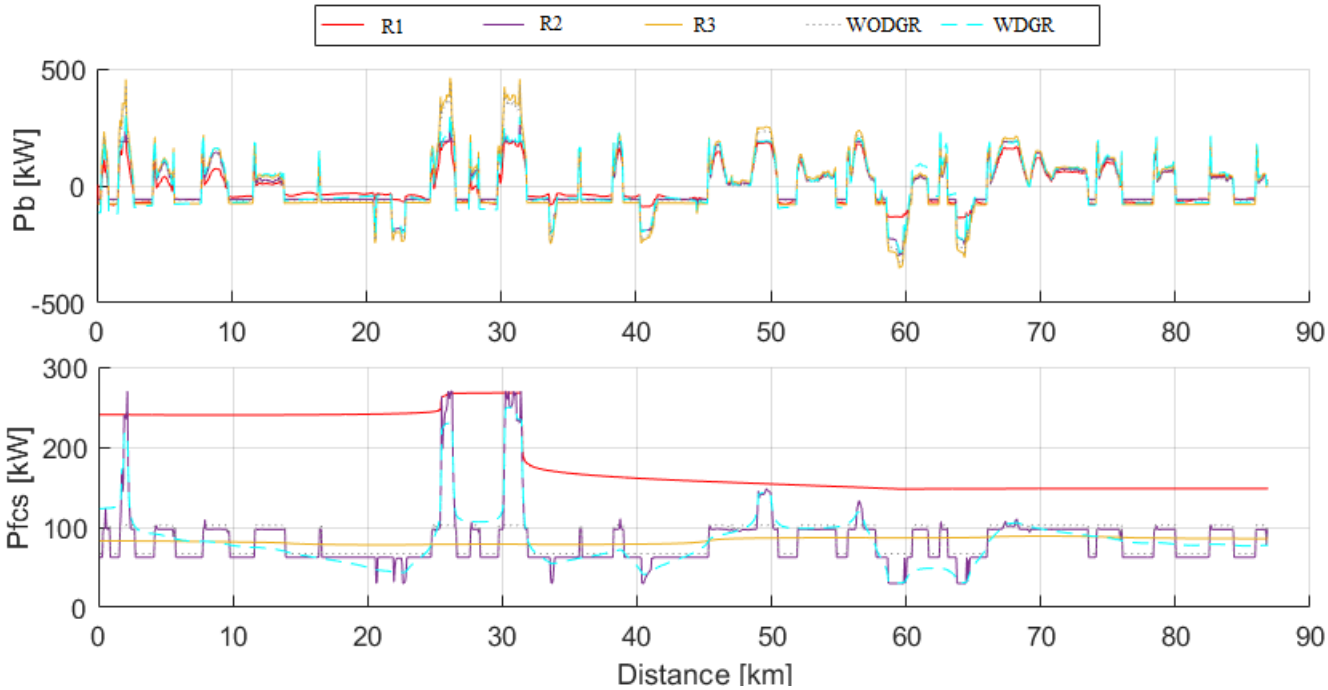

Figure 5.14: *A comparison of the optimal power vectors for different combinations of the cost terms.*

5.3 Sensitivity Analysis of Cost and Horizon Length

Figure 5.15 shows the effects of varying c_{H2}, c_f and c_b with $\pm 5\%$ on the total cost.

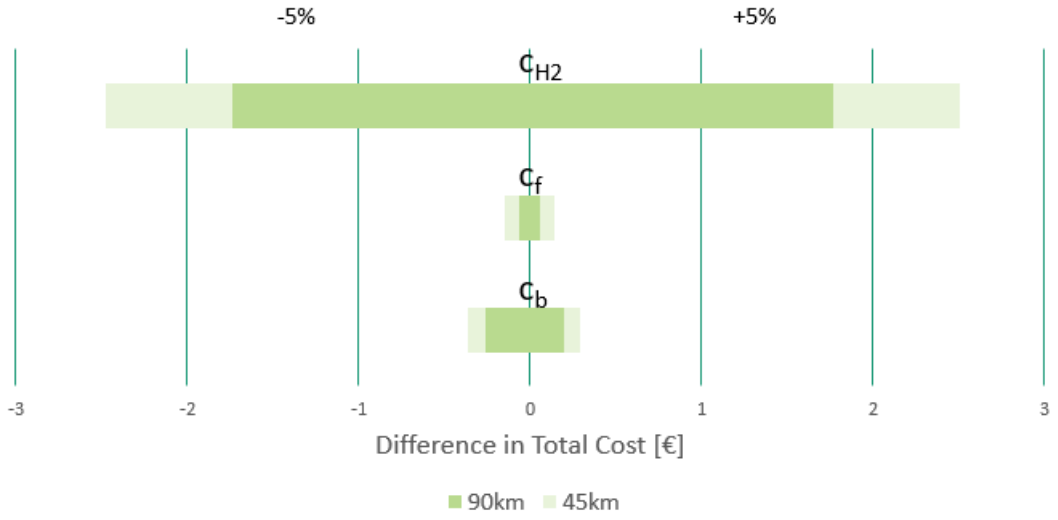

Figure 5.15: *The effects of changing c_{H2}, c_f and c_b with $\pm 5\%$ and the effects of halving the horizon on the total cost. The analysis was performed on WDGR and the base-value, 0 in the graph, is the resulting Total Cost for WDGR with the relevant horizon length.*

6 Discussion

This chapter provides a discussion of the results presented in the previous chapter.

6.1 Battery Degradation: Problems with the Plant Model

As already mentioned the Plant Model of the battery degradation is closely based on the model presented in Hu et al. (2020) [18]. However, not all needed numerical values were available for this thesis, so the final model used has a mixture of numerical data from Hu et al. and Volvo. This is, of course, not optimal and essentially makes the controller think the Volvo battery will die about 3 times as early as Hu's battery. In reality, when comparing e.g. the nominal capacity and other values, the Volvo battery would be expected to have a better lifetime; the issues lies, of course, with the missing numerical values.

As already mentioned, this means that all results presented in this thesis assume the battery degradation is faster than it probably is in reality. The issue can easily be resolved by Volvo updating the software with the correct numerical values.

6.2 Battery Degradation: Plant Model vs. Controller Model

As mentioned in Chapter 4 the Plant Models for the degradation, especially for the battery, needed to be simplified in the controller to fit the QP formulation. Figure 5.4 plots the used battery degradation values for both cases; the capacity fade plant model (blue) and the piece-wise linear approximation used in the controller (red). As can be seen, the two models match up well for low absolute values of battery cell power, but deviate for higher values especially between 400-600W.

The difference is also seen in the resulting $\mathbb{SOH}_\mathrm{b}$ plot. Figure 5.5 shows the $\mathbb{SOH}_\mathrm{b}$ development for WDGR (further explained in the next Section) over the horizon of 90km, both for the Plant Model and the Controller Model. As can be seen, the more complicated Plant Model calculates a bigger battery degradation state-of-health with the largest difference between the two being 0.159%. The Control Model's error is accumulative in nature since each $\mathbb{SOH}_\mathrm{b}[k]$ inherits the error from its predecessor $\mathbb{SOH}[k-1]$. This may seem like a big issue, though one easily solved by introducing feedback between the plant model and the controller, but it is important to remember that the controller minimises the *difference* between $\mathbb{SOH}_\mathrm{b}[k]$ and $\mathbb{SOH}_\mathrm{b}[k-1]$ (also called $z_{\mathbb{b}}$, see Equation 4.8), so while the error in the plotted $\mathbb{SOH}$ is accumulative in nature, the actual error of the value used in the objective function is not.

6.3 Modified Controller Without Degradation (WODGR)

Figure 5.6 shows a resulting plot from the WODGR. As can be seen, over the horizon of 90km, the demand from the EM, $\boldsymbol{P}_\mathrm{ref}$, is met by the sum of $\mathbb{P}_\mathrm{f}$ and $\mathbb{P}_\mathrm{b}$.

As seen both in Figure 5.6 and 5.8 the most common behaviour is when $\boldsymbol{P}_\mathrm{ref}$ is 0 and the Power Split decides to have $\mathbb{P}_\mathrm{f}$ be 60kW and charge the battery with the corresponding -60kW. The other most common mode for the fuel cell is at a slightly higher plateau of ca 100kW. $\mathbb{P}_\mathrm{f}$ mostly alternates between these two values, 60kW and 100 kW, while the battery power varies more and acts as a buffer to meet the variations in $\boldsymbol{P}_\mathrm{ref}$. The battery $\mathbb{SOC}$ varies between it is allowed minimal and maximal value and has three distinctive peaks.

The computational time for all runs preformed in this thesis is short, less than 2s. Variations in computational time are therefore assumed to be too low to be essential for the results.

6.4 Comparison: Modified Controller With & Without Degradation

Table 5.1 shows, among other things, the main differences between the WODGR and WDGR. In both cases, over the distance of 90km, the cost of the consumption of H_2 is the largest, which is to be expected since the degradation over such a short distance should be small enough to take out the larger cost of the components. Despite c_f being larger than c_b the total term for the cost of the battery degradation is about 10 times larger than the cost of the fuel cell. This is unexpected and not a common result from literature, where the results commonly show the fuel cell degradation cost is larger than the battery degradation cost [13][18][38]. The reason why this thesis shows the opposite is probably due to the model assuming the battery deteriorates a lot faster than it actually does, as explained in Section 6.1. Keeping this in mind, the high battery degradation cost makes sense as does the results from WDGR, which propose using the fuel cell more strenuously in order to save more battery life.

Looking at Figure 5.11, the more strenuous use of the fuel cell can be seen in the higher peaks and valleys for WDGR compared to the WODGR. The battery power of WDGR instead has corresponding lower peaks.

Another difference between WDGR and the WODGR can be seen from Figures 5.7, 5.9 and 5.12. They all show that the optimal $\mathbb{P}_\mathrm{f}$ for WDGR has more, but smaller transients instead of alternating between the two modes described in Section 6.3 and seen in Figures 5.6 and 5.8. Comparing Figure 5.7 to 5.6 it is possible to see the $\mathbb{P}_\mathrm{f}$ in orange having smoother transients in WDGR. The $\mathbb{SOC}$ development still has three peaks in the WDGR, but the depth of discharge is smaller than for the WODGR. The density plots, Figures 5.9 and 5.8, are drastically different, clearly showcasing the difference between $\mathbb{P}_\mathrm{f}$ favouring two modes and having more, but smaller variations. Figure 5.12 showcases these differences in variations even more explicitly, showing and comparing the frequency of the different transients in the optimal solution.

6.5 Comparison: Other Combinations of the Cost Terms

Excluding different parts of the objective function can help give understanding to how different terms effect the optimal behaviour. R3 and R4 exclude the cost of fuel cell and battery degradation respectively, while R2 excludes the cost of H_2-consumption. Returning to Table 5.1 one can compare the results of these experiments to the WODGR and WDGR. The data is also complemented by Figure 5.14 which shows the optimal power distribution for the given horizon.

Starting with analysing R2, with an objective function that only includes degradation, it can be noted that this strategy is not advised as it is ca 50€ more expensive than the others. Looking at Figure 5.14 it can also be noted that this experiment also has a $\mathbb{P}_\mathrm{f}$ most different from the others, with a higher overall operating region than the other strategies. As already stated, the H_2 cost is not negligible, so this observation is not surprising.

Except for R2, the H_2-cost is around 35€ for all other runs and the differences in total cost stem from the differences in degradation. Here it is again important to remember that the results for the battery degradation are skewed due to the reasons described in Section 6.1 and thus have a higher impact on the behaviour than expected. This is e.g. clear from the fact that as soon as the battery degradation term is included in the objective function (i.e. R2, R3 and R1) the battery degradation is lowered from the WODGR and, looking at Figure 5.14, the behaviour of $\mathbb{P}_\mathrm{b}$ is set to have lower peaks and valleys in order to save battery health.

The reason why the lowest battery degradation is obtained from R2 and not R3 is due to the H_2-consumption dominating the cost and thus pushing the battery to behave sub-optimally.

Excluding the battery degradation (R4) leads to a very small fuel cell degradation with an almost constant $\mathbb{P}_{\mathrm{f}}$.

6.6 Sensitivity Analysis of Cost and horizon length

As already hinted at, Section 6.5, the controller is most sensitive to the hydrogen cost since this term dominates the cost over the short horizon. Varying c_{H2} with $\pm$ 5% results in a difference of ca 1.75€ for the horizon of 90km. If the horizon is halved to 45km, this sensitivity increases to ca 2.5€.

Halving the horizon makes the model more sensitive when it comes to c_{b} and c_{f} as well. Also, once again the larger sensitivity to the battery degradation can be observed.

6.7 Comparison: Original Controller vs. Modified Controller

As explained in Chapter 4, the difference between the Modified and the Original Controller is exchanging the heuristic constraints on the usage with degradation costs. As could be expected, the HEUR and WODGR show very similar results: their objective functions are most similar since they do not include the degradation terms. What is also expected is that the HEUR has slightly less fuel cell degradation and a slightly higher fuel cost: compared to the WODGR which has no limitations on the fuel cell usage in regards to degradation, the Original Controller has some heuristic limits designed to lower fuel cell degradation.

That the WODGR and the HEUR are very similar can also be seen from how similar Figures 5.10 and 5.8 are.

When looking at the frequency of the transients in Figure 5.13 and comparing it to Figure 5.12, the most important thing to note is that the HEUR has the highest percentage of $\Delta\mathbb{P}_{\mathrm{f}} = 0kW$ compared to WODGR and WDGR. This makes sense, as the objective function includes a term for minimising $\Delta\mathbb{P}_{\mathrm{f}}$. However, when looking at the extreme values in the plots the following can be observed: the largest transient at -36kW is from the WODGR, the second largest at -17kW is from the HEUR and lastly, the WDGR's largest transient is a mere -4kW. So while $\Delta\mathbb{P}_{\mathrm{f}}$ for the HEUR spends more time being 0 than for the WDGR, its maximal value is still ten times larger than for the WDGR. As already observed, the WDGR introduces more smaller transients of ca $\pm 3kW$ and removes the bigger transients.

To summarise, having some heuristic limits to lessen the degradation (HEUR) is better than having none at all (WODGR), but including actual degradation models in the controller (WDGR) is better still.

6.8 Additional Reflections

Using a QP formulation to model the nonlinear degradations is probably defendable. If this thesis is to be believed, it improves the Original Controller a lot, even if not all the nonlinear behaviour is captured. There are also ways of defining the battery degradation and objective function in such a way that the Control Model does not need to be piece-wise linearised. If the degradation is e.g. approximated by a second degree polynomial, it can be included in the objective function, which can be of the second order, instead of in the constraints, which need to be linear. Furthermore, to capture more of the nonlinear behaviour, several second degree polynomials could be used for a piece-wise second degree approximation. While the fuel cell degradation model in this thesis is very rudimentary, the fact that Fonesca (2013) [15] models fuel cell degradation as a second degree polynomial also supports the claim that a QP formulation should be sufficient. It would certainly be interesting to compare the model used by Fonesca to the model used by Wang et al. (2019) [38] and, perhaps, combine them.

The issue of capturing the way degradation effects efficiency is, at the time of writing, still in the air. Neither in the Original nor in the Modified software is this addressed, since η_b is kept constant and the fuel cell efficiency is not touched upon in this thesis. However, it is also not included in Hu et al. (2020) [18] or in Feng et al. (2020) [13] and, while Wang et al. do include it for the fuel cell they do not seem to do so for the battery, so this seems to be an area that could do with more research. There are different ways the issue could be approached. A simple periodical update of the efficiency factor and/or the polarisation curve, similar to what is done by Wang et al. could do the trick. Another way would be including equivalent circuits for both the battery and the fuel cell. For the battery this would be more straight forward, as a consensus on which circuit captures enough of the behaviour seems to have been reached. Using the circuit to capture efficiency instead of η_b, also opens up for defining $\mathbb{SOH}_b$ as a combination of power and capacity State-of-Health as Diao et al. (2017) [7] suggest.

A concern raised during the research phase of this thesis was whether the degradation changes over the short examined horizon were too small and if they would be within the error margins dictated by noise. This thesis cannot answer that, since the model used is deterministic in nature and also because of the numerical issues that skew the values of the degradation. However, the examined literature seems to argue that since the cost factors c_b and c_f are relatively big, this is not an issue.

7 Conclusion

Condensed down, one can say this thesis compares three different controllers: one minimising only the H_2-consumption (WODGR), one minimising the H_2-consumption and the degradation of electrochemical components (WDGR) and one minimising the H_2-consumption but including heuristic constraints to limit the fuel cell degradation (HEUR). The HEUR shows very similar results to the WODGR, i.e. the heuristics in the HEUR, according to this thesis, do not capture the degradation sufficiently or at least not as well as the WDGR. It is, however, important to note that issues with the with the battery degradation in the WDGR (see Sections 6.1 and 5.1) make the WDGR overestimate the cost of battery degradation, thus it is impossible to say if this reasoning is correct without updating the numerical data. Though the cost of H_2-consumption dominates the cost over the short examined horizon of 90km, both literature and the results of experiments run in this thesis suggest that including some form of restraints or costs relating to the wear on the electrochemical components, be it heuristic limitations on the use (HEUR) or models tracking and minimising the degradation (WDGR), does lower the TCO.

Returning to the Research Questions presented in Section 1.1, the following answers can be sketched out:

- How is the degradation of the BP and the FCS to be included in the Power Split Controller?

  According to the research done in this thesis, a QP formulation of the optimisation problem should be sufficient. Herein, the battery degradation is modelled by a capacity fade model (Equation (3.11)) and the fuel cell degradation is modelled by setting a high cost for high, low and transient load. Both these could be improved upon and especially the fuel cell degradation is heavily dependant on experimental data.

- How does changing the cost of degradation affect the performance of the vehicle?

  Including the degradation models smooths out the transients in fuel cell power ($\Delta \mathbb{P}_{\mathrm{f}}$) and removes the larger transients.

- Is including the cost of degradation relevant for future research?

  Both literature and this thesis conclude that including degradation in the objective function in the Power Split Controller generate savings over time. Together with a PR push to make consumers aware of the advantages of a low TCO, would be a benefit for companies such as Volvo as well.

8 Appendix

8.1 Battery Degradation

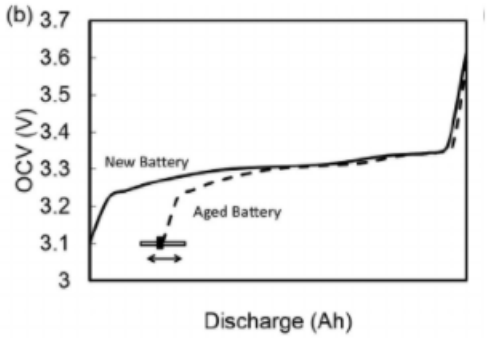

Figure 8.1: *The relationship between U^{id} (OCV) and capacity (discharge in Ah) for a new and old battery according to [35]. (Image from Tong et al. (2015) [35])*

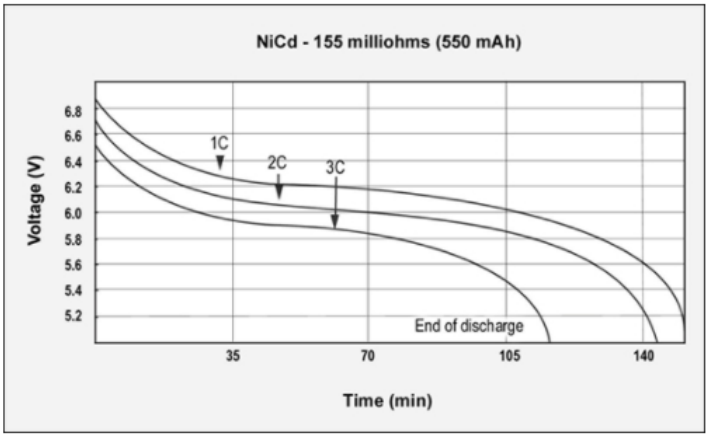

Figure 3: GSM discharge pulses at 1, 2, and 3C with resulting talk-time
The capacity of the NiCd battery is 113%; the internal resistance is 155mΩ. 7.2V pack.

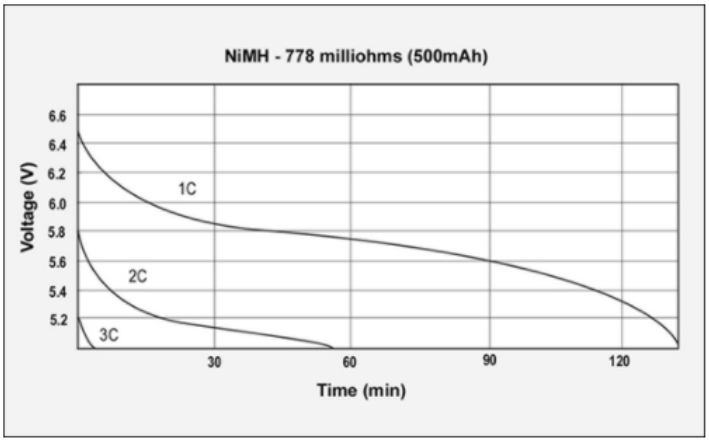

Figure 4: GSM discharge pulses at 1, 2, and 3C with resulting talk-time
The capacity of the NiMH battery is 94%, the internal resistance is 778mΩ. 7.2V pack

Figure 8.2: *The two figures show the difference between a high and low internal resistance. Note that the higher resistance (second image, Figure 4) has a much shorter runtime, especially for high discharge rates (3C). (Image from Battery University [36])*

8.2 Fuel Cell Degradation

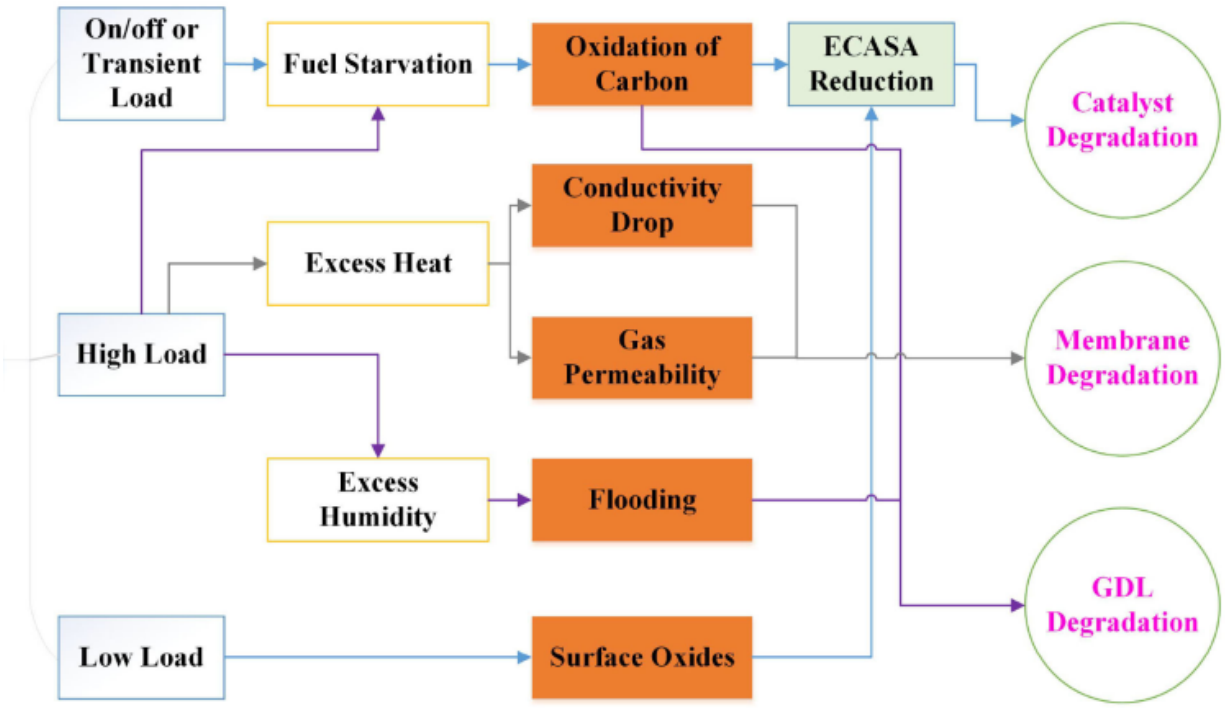

Figure 8.3: *The different types of fuel cell degradation resulting from strenuous use. (Image from Hu et al. (2020) [18])*

References

[1] E. E. Agency. *Indicator Assessment: Greenhouse gas emissions from transport in Europe*. 2020. URL: https://www.eea.europa.eu/data-and-maps/indicators/transport-emissions-of-greenhouse-gases-7/assessment. (Accessed: 2021-01-22).

[2] P. Atkins, L. Jones, and L. Laverman. *Chemical Principles: The Quest for Insight*. Vol. Sixth Edition. W.H. Freeman and Company, New York, 2013. ISBN: 1-4641-2467-1.

[3] I. Baghdadi et al. Lithium battery aging model based on Dakin's degradation approach. *Journal of Power Sources* **325** (2016), 273–285. ISSN: 0378-7753. DOI: https://doi.org/10.1016/j.jpowsour.2016.06.036. URL: http://www.sciencedirect.com/science/article/pii/S0378775316307388.

[4] B. Balagopal and M.-Y. Chow. "The state of the art approaches to estimate the state of health (SOH) and state of function (SOF) of lithium Ion batteries". July 2015, pp. 1302–1307. DOI: 10.1109/INDIN.2015.7281923.

[5] A. Barré et al. *A review on lithium-ion battery ageing mechanisms and estimations for automotive applications*. Journal of Power Sources, Elsevier. v:241, p:680-689 http://fs.fish.govt.nz/Page.aspx?pk=7&sc=SUR. (Accessed: 2020-12-13). 2013.

[6] I. Buchmann. *Battery University: Capacity Loss*. 2019. URL: https://batteryuniversity.com/learn/article/capacity_loss. (Accessed: 2021-01-22).

[7] W. Diao et al. Energy state of health estimation for battery packs based on the degradation and inconsistency. *Energy Procedia* **142** (2017). Proceedings of the 9th International Conference on Applied Energy, 3578–3583. ISSN: 1876-6102. DOI: https://doi.org/10.1016/j.egypro.2017.12.248. URL: http://www.sciencedirect.com/science/article/pii/S1876610217359829.

[8] A. L. Duigou and A. Smatti. On the comparison and the complementarity of batteries and fuel cells for electric driving. *International Journal of Hydrogen Energy* **39**.31 (2014), 17873–17883. ISSN: 0360-3199. DOI: https://doi.org/10.1016/j.ijhydene.2014.08.077. URL: http://www.sciencedirect.com/science/article/pii/S0360319914023775.

[9] S. Ebbesen and L. Guzzella. "Trade-Off Between Fuel Economy and Battery Life for Hybrid Electric Vehicles". Vol. 2. Jan. 2011. DOI: 10.1115/DSCC2011-5950.

[10] S. Ebbesen and L. Guzzella. Trade-Off Between Fuel Economy and Battery Life for Hybrid Electric Vehicles. Dynamic Systems and Control Conference **ASME 2011 Dynamic Systems and Control Conference and Bath/ASME Symposium on Fluid Power and Motion Control, Volume 2** (Oct. 2011), 217–223. DOI: 10.1115/DSCC2011-5950. eprint: https://asmedigitalcollection.asme.org/DSCC/proceedings-pdf/DSCC2011/54761/217/2767181/217_1.pdf. URL: https://doi.org/10.1115/DSCC2011-5950.

[11] European and Commission. *Mobility and transport: Road Safety: Heavy goods vehicles*. 2020. URL: https://ec.europa.eu/transport/road_safety/specialist/knowledge/vehicle/safety_design_needs/heavy_goods_vehicles_en. (Accessed: 2020-09-17).

[12] W. Feng and M. Figliozzi. An economic and technological analysis of the key factors affecting the competitiveness of electric commercial vehicles: A case study from the USA market. *Transportation Research Part C: Emerging Technologies* **26** (2013), 135–145. ISSN: 0968-090X. DOI: https://doi.org/10.1016/j.trc.2012.06.007. URL: http://www.sciencedirect.com/science/article/pii/S0968090X12000897.

[13] Y. Feng and Z. Dong. Integrated design and control optimization of fuel cell hybrid mining truck with minimized lifecycle cost. *Applied Energy* **270** (2020), 115164. ISSN: 0306-2619. DOI: https://doi.org/10.1016/j.apenergy.2020.115164. URL: http://www.sciencedirect.com/science/article/pii/S0306261920306760.

[14] K. Field. *Clean Technica: Toyota Mirai Hydrogen fuel cell Vehicle Review*. 2018. URL: https://cleantechnica.com/2018/06/16/toyota-mirai-hydrogen-fuel-cell-vehicle-review-cleantechnica-exclusive/. (Accessed: 2020-09-17).

[15] R. Fonseca. Optimisation du dimensionnement et de la gestion d'énergie d'un véhicule à pile à combustible intégrant les contraintes de dynamiques et de durabilité (Oct. 2013).

[16] T. Ghandriz et al. Impact of automated driving systems on road freight transport and electrified propulsion of heavy vehicles. *Transportation Research Part C: Emerging Technologies* **115** (2020), 102610. ISSN: 0968-090X. DOI: https://doi.org/10.1016/j.trc.2020.102610. URL: http://www.sciencedirect.com/science/article/pii/S0968090X18311574.

[17] O. Gröger, H. Gasteiger, and J.-P. Suchsland. Review—Electromobility: Batteries or Fuel Cells? *Journal of The Electrochemical Society* **162** (2015).

[18] X. Hu et al. Cost-Optimal Energy Management of Hybrid Electric Vehicles Using Fuel Cell/Battery Health-Aware Predictive Control. *IEEE Transactions on Power Electronics* **35**.1 (2020), 382–392.

[19] X. Hu et al. Longevity-conscious dimensioning and power management of the hybrid energy storage system in a fuel cell hybrid electric bus. *Applied Energy* **137**.C (2015), 913–924. DOI: 10.1016/j.apenergy.2014.0. URL: https://ideas.repec.org/a/eee/appene/v137y2015icp913-924.html.

[20] P. V. J. Lungren M. Rönnqvist. *Optimization*. Studentlitteratur AB, Lund, 2010. ISBN: 9789144053080.

[21] M. Jouin et al. PEMFC aging modeling for prognostics and health assessment. *IFAC-PapersOnLine* **48**.21 (2015). 9th IFAC Symposium on Fault Detection, Supervision andSafety for Technical Processes SAFEPROCESS 2015, 790–795. ISSN: 2405-8963. DOI: https://doi.org/10.1016/j.ifacol.2015.09.623. URL: http://www.sciencedirect.com/science/article/pii/S2405896315017528.

[22] J.-H. Kim, H.-J. Kim, and S.-H. Yoo. Willingness to pay for fuel-cell electric vehicles in South Korea. *Energy* **174** (2019), 497–502. ISSN: 0360-5442. DOI: https://doi.org/10.1016/j.energy.2019.02.185. URL: http://www.sciencedirect.com/science/article/pii/S0360544219303913.

[23] D. Kolodziejak et al. An optimization and analysis framework for TCO minimization of plug-in hybrid heavy-duty electric vehicles. English. *IFAC-PapersOnLine* **52**.5 (2019). 9th IFAC Symposium on Advances in Automotive Control, (AAC2019), 9th AAC 2019 ; Conference date: 24-06-2019 Through 27-06-2019, 484–491. ISSN: 2405-8963. DOI: 10.1016/j.ifacol.2019.09.077. URL: http://www.ifac-control.org/events/advances-in-automotive-control-9th-aac-2019.

[24] S. Lazarou et al. "PEM fuel cell equivalent circuit models: A review". June 2008.

[25] W. Li et al. Willingness to pay for hydrogen fuel cell electric vehicles in China: A choice experiment analysis. *International Journal of Hydrogen Energy* (2020). ISSN: 0360-3199. DOI: https://doi.org/10.1016/j.ijhydene.2020.01.046. URL: http://www.sciencedirect.com/science/article/pii/S0360319920301361.

[26] J. Löfberg. "YALMIP : A Toolbox for Modeling and Optimization in MATLAB". *In Proceedings of the CACSD Conference*. Taipei, Taiwan, 2004.

[27] S. Ma et al. Fuel cell-battery hybrid systems for mobility and off-grid applications: A review. *Renewable and Sustainable Energy Reviews* **135** (2021), 110119. ISSN: 1364-0321. DOI: https://doi.org/10.1016/j.rser.2020.110119. URL: http://www.sciencedirect.com/science/article/pii/S136403212030410X.

[28] H. Meng and Y.-F. Li. A review on prognostics and health management (PHM) methods of lithium-ion batteries. *Renewable and Sustainable Energy Reviews* **116** (2019), 109405. ISSN: 1364-0321. DOI: https://doi.org/10.1016/j.rser.2019.109405. URL: http://www.sciencedirect.com/science/article/pii/S1364032119306136.

[29] P. Pei et al. Nonlinear methods for evaluating and online predicting the lifetime of fuel cells. *Applied Energy* **254** (2019), 113730. ISSN: 0306-2619. DOI: https://doi.org/10.1016/j.apenergy.2019.113730. URL: http://www.sciencedirect.com/science/article/pii/S0306261919314175.

[30] H. Perez et al. Optimal Charging of Li-Ion Batteries via a Single Particle Model with Electrolyte and Thermal Dynamics. *Journal of The Electrochemical Society* **164** (June 2017), A1679–A1687. DOI: 10.1149/2.1301707jes.

[31] P. Pettersson and C. tekniska högskola. Institutionen för mekanik och maritima vetenskaper. *Operating Cycle Representations for Road Vehicles*. Doktorsavhandlingar vid Chalmers tekniska högskola. Chalmers University of Technology, 2019. ISBN: 9789179052102. URL: https://books.google.se/books?id=bCJ4zQEACAAJ.

[32] J. Pukrushpan. Modeling and Control of Fuel Cell Systems and Fuel Processors (Jan. 2003).

[33] K. Runtz and M. Lyster. "Fuel cell equivalent circuit models for passive mode testing and dynamic mode design". *Canadian Conference on Electrical and Computer Engineering, 2005.* 2005, pp. 794–797. DOI: 10.1109/CCECE.2005.1557048.

[34] K. Runtz and M. Lyster. "Fuel cell equivalent circuit models for passive mode testing and dynamic mode design". *Canadian Conference on Electrical and Computer Engineering, 2005.* 2005, pp. 794–797. DOI: 10.1109/CCECE.2005.1557048.

[35] S. Tong, M. Klein, and J. Park. On-line Optimization of Battery Open Circuit Voltage for Improving State-of-Charge and Sate-of-Health Estimation. *Journal of Power Sources* **293** (Mar. 2015). DOI: 10.1016/j.jpowsour.2015.03.157.

[36] I. B. (University). *Battery University: Rising Internal Resistance*. 2019. URL: https://batteryuniversity.com/learn/article/rising_internal_resistance. (Accessed: 2020-12-13).

[37] J. Wang et al. Cycle-life model for graphite-LiFePO4 cells. *Journal of Power Sources* **196**.8 (2011), 3942–3948. ISSN: 0378-7753. DOI: https://doi.org/10.1016/j.jpowsour.2010.11.134. URL: http://www.sciencedirect.com/science/article/pii/S0378775310021269.

[38] Y. Wang et al. Power management system for a fuel cell/battery hybrid vehicle incorporating fuel cell and battery degradation. *International Journal of Hydrogen Energy* **44**.16 (2019), 8479–8492. ISSN: 0360-3199. DOI: https://doi.org/10.1016/j.ijhydene.2019.02.003. URL: http://www.sciencedirect.com/science/article/pii/S0360319919305014.

[39] G. Wu, A. Inderbitzin, and C. Bening. Total cost of ownership of electric vehicles compared to conventional vehicles: A probabilistic analysis and projection across market segments. *Energy Policy* **80** (2015), 196–214. ISSN: 0301-4215. DOI: https://doi.org/10.1016/j.enpol.2015.02.004. URL: http://www.sciencedirect.com/science/article/pii/S0301421515000671.

[40] Q. Xun, S. Lundberg, and Y. Liu. Design and experimental verification of a fuel cell/supercapacitor passive configuration for a light vehicle. *Journal of Energy Storage* **33** (2021). DOI: http://dx.doi.org/10.1016/j.est.2020.102110.

[41] Q. Xun et al. Drive Cycle Energy Efficiency of Fuel Cell/Supercapacitor Passive Hybrid Vehicle System. *IEEE Transactions on Industry Applications* **57**.1 (2021), 894–903. DOI: 10.1109/TIA.2020.3035551.

[42] S. H. Zak. *An Introduction to Model-based Predictive Control (MPC)*. 2017. URL: https://engineering.purdue.edu/~zak/ECE680/MPC_handout.pdf. (Accessed: 2021-01-22).

[43] X. Zhang et al. A novel quantitative electrochemical aging model considering side reactions for lithium-ion batteries. *Electrochimica Acta* **343** (2020), 136070. ISSN: 0013-4686. DOI: https://doi.org/10.1016/j.electacta.2020.136070. URL: http://www.sciencedirect.com/science/article/pii/S001346862030462X.